Multi-omic analyses reveal a role for mammalian CIC in cell cycle regulation and mitotic fidelity

Yuka Takemon[1,2,*], Veronique G. LeBlanc[2,*], Jungeun Song[2], Susanna Y. Chan[2], Stephen Dongsoo Lee[2], Diane L. Trinh[2], Shiekh Tanveer Ahmad[3,4,5], William R. Brothers[2], Richard D. Corbett[2], Alessia Gagliardi[2], Annie Moradian[2], J Gregory Cairncross[4,6], Stephen Yip[7,8], Samuel A.J.R. Aparicio[7,8], Jennifer A. Chan[3,4,5], Christopher S. Hughes[7], Gregg B. Morin[2,9], Sharon M. Gorski[2,10], Suganthi Chittaranjan[2], Marco A. Marra[2,9]

[1] Genome Science and Technology Graduate Program, University of British Columbia, Vancouver, Canada
[2] Canada's Michael Smith Genome Sciences Centre, BC Cancer Research Institute, Vancouver, Canada
[3] Department of Pathology & Laboratory Medicine, University of Calgary, Calgary, Canada
[4] Arnie Charbonneau Cancer Institute, University of Calgary, Calgary, Canada
[5] Alberta Children's Hospital Research Institute, University of Calgary, Calgary, Canada
[6] Department of Clinical Neurosciences, University of Calgary, Calgary, Canada
[7] Department of Molecular Oncology, BC Cancer Research Institute, Vancouver, Canada
[8] Department of Pathology and Laboratory Medicine, University of British Columbia, Vancouver, Canada
[9] Department of Medical Genetics, University of British Columbia, Vancouver, Canada
[10] Department of Molecular Biology and Biochemistry, Simon Fraser University, Burnaby, Canada

* These authors contributed equally to this work

Running title: Multi-omic CIC analyses reveal link to cell cycle

Abstract

CIC encodes a transcriptional repressor that is inactivated by loss-of-function mutations in several cancer types, indicating that it may function as a tumor suppressor. Recent studies have indicated that CIC may regulate cell cycle genes in humans; however, a systematic investigation of this proposed role has not yet been reported. Here, we used single-cell RNA sequencing to show that inactivation of CIC in human cell lines correlated with transcriptional dysregulation of genes involved in cell cycle control. We also mapped CIC's protein-protein and genetic interaction networks, identifying interactions between CIC and members of the Switch/Sucrose Non-Fermenting (SWI/SNF) complex as well as revealing novel candidate interactions between CIC and cell cycle regulators. We further showed that CIC loss was associated with an increased frequency of mitotic defects in human cell lines and in a mouse model. Our study thus positions CIC as a cell cycle regulator and indicates that CIC loss can lead to mitotic errors, consistent with CIC's emerging role as a tumor suppressor of relevance in several cancer contexts.

Keywords

CIC, cell cycle, single-cell sequencing, protein-protein interaction, genetic interaction network

Introduction

Capicua (CIC) is a transcriptional repressor that is impacted by somatic mutations or rearrangements in several cancer types, including undifferentiated small round cell sarcomas (~60% frequency) (Haidar et al. 2015), oligodendrogliomas (~50-80%) (Bettegowda et al. 2011; Yip et al. 2012), gastric adenocarcinomas (~9%) (The Cancer Genome Atlas Research Network, 2014), endometrial carcinomas (~7%) (The Cancer Genome Atlas Research Network, 2013), and melanomas (~8%) (Cerami et al. 2012; Gao et al. 2013). CIC loss has also been linked to prostate cancer (Choi et al. 2015), lung cancer (Okimoto et al. 2017), and T-cell lymphoblastic leukemia/lymphoma (Simon-Carrasco et al. 2017; Tan et al. 2018). *CIC* alterations and/or loss of CIC activity have been associated with inferior survival outcomes in several cancer types (Chan et al. 2014; Gleize et al. 2015; Specht et al. 2014; Antonescu et al. 2017) and with aggressive phenotypes such as increased metastasis (Okimoto et al. 2017) and resistance to kinase inhibitors (Liao et al. 2017; Wang et al. 2017; Hashiba et al. 2020). Together, these observations are compatible with the notion that CIC functions as a tumor suppressor across cancer types.

The cancer-promoting properties observed in cells with disrupted CIC activity have been explained, at least in part, by the de-repression of one or more of its known target genes, such as the ETS transcription factors *ETV1*, *ETV4*, and *ETV5* (Choi et al. 2015; Okimoto et al. 2017; Simon-Carrasco et al. 2017). An analysis of data from The Cancer Genome Atlas (TCGA) consortium showed that loss of CIC was also associated with dysregulated expression of several genes associated with mitosis — including *AURKA*, *CDK4*, and *BUB1* — across multiple cancer types (Wong et al. 2019). This observation raised the possibility that CIC may play a role in cell cycle regulation. Consistent with this hypothesis, Cic was shown to inhibit proliferation in *Drosophila* tissues through transcriptional repression of cell cycle genes, including String/Cdc25 and Cyclin E (Simón-Carrasco et al. 2018). However, the extent of CIC's potential role in the cell cycle has not yet been fully elucidated, especially in mammalian disease models. Given that somatic *CIC* alterations are found in multiple cancer types and that CIC is also understood to

play a role in the development and physiology of multiple organ systems (e.g. brain and lung development, T-cell differentiation (Lee 2020)), a more thorough understanding of CIC function could have important implications in contexts where CIC appears relevant.

To further explore the possible roles CIC might play in cell cycle regulation, we used multi-omics and bioinformatics approaches to map CIC's transcriptional regulatory network and its proteomic and genetic interaction networks in human cell lines. Through this work, we introduce a potentially new role for CIC in regulating mitotic integrity and cell cycle progression. Using single-cell RNA sequencing (scRNA-seq), we show that loss of CIC is associated with dysregulated expression of cell cycle genes at distinct cell cycle phases. We demonstrate physical interactions between CIC and proteins involved in cell cycle functions, as well as between CIC and members of the Switch/Sucrose Non-Fermenting (SWI/SNF) complex, and find that *CIC* is predicted to genetically interact with genes involved in mitotic regulation and chromosome segregation. Finally, through analyses of human cell lines and a *Cic* knockout mouse model, we demonstrate that loss of CIC/Cic is associated with an increased frequency of mitotic defects. Overall, our work describes the effect of CIC loss on regulators of cell cycle progression and mitotic integrity, thus providing new insights into CIC's potential role(s) in cancers.

Results

Loss of CIC is associated with dysregulated expression of cell cycle genes

Given that Cic regulates cell cycle progression in *Drosophila* (Simón-Carrasco et al. 2018) and that human tumors with *CIC* alterations show dysregulated expression of cell cycle regulators (Wong et al. 2019), we set out to profile the effects of CIC loss on human transcriptome regulation using isogenic *CIC* knockout (CIC^{KO}) cell lines derived from an immortalized normal human astrocyte (NHA) line (Sonoda et al. 2001; LeBlanc et al. 2017). The expression of cell cycle regulators is tightly regulated and often

changes dynamically with the cell cycle (Liu et al. 2017); furthermore, dysregulated expression of dynamically expressed genes may not be detectable in asynchronous bulk cell populations, and synchronization through either chemical or physical means can introduce confounding artifacts (Cooper 2003; Hsiao et al. 2020). We therefore performed scRNA-seq on asynchronous *CIC* wild type (parental NHA line, NHA-*CIC*^{WT}) and *CIC*^{KO} (NHA-*CIC*^{KO1} and NHA-*CIC*^{KO2} lines) cells, and then used the data to assign cells to cell cycle phases. In this way, we sought to understand the transcriptional profiles of CIC-proficient and CIC-deficient cells at different phases of the cell cycle.

We scored cells for defined cell cycle phases using approaches described by Macosko et al. (2015) (Supplemental Figure S1a; Methods). Assigning cells to the phase for which they scored highest, we found that the proportions of *CIC*^{KO} cells assigned to the G2/M phase (21% in NHA-*CIC*^{KO1} and 20% in NHA-*CIC*^{KO2}) were nearly 2-fold higher than the proportion of *CIC*^{WT} cells assigned to G2/M (12%; Figure 1a). The *CIC*^{KO} lines also contained ~2-3-fold lower proportions of cells assigned to the M/G1 phase (10% in NHA-*CIC*^{KO1} and 15% in NHA-*CIC*^{KO2}) compared to the parental *CIC*^{WT} line (29%), while more *CIC*^{KO} cells were assigned to the G1/S phase, especially in the NHA-*CIC*^{KO1} line (41% in NHA-*CIC*^{KO1} and 31% in NHA-*CIC*^{KO2} vs 26% in NHA-*CIC*^{WT}). These observations could reflect G2/M and G1/S transition delays in *CIC*^{KO} cells, leading to abnormal accumulations of cells at these stages.

To explore whether loss of CIC was associated with gene expression changes in cells at different phases of the cell cycle, we then used the scRNA-seq data to perform differential expression analyses comparing *CIC*^{WT} and *CIC*^{KO} cells assigned to G2, G2/M, M/G1, G2/S, and S phases (Supplemental Table S1). Since it can be challenging to differentiate between cells in the process of transitioning between phases, we avoided such cells by restricting our analysis to the top 50% of cells in each cell line with the highest scores for each phase (486-1,191 cells per phase, mean 773; Methods). As expected, canonical CIC targets, such as *ETV4* and *ETV5,* displayed significantly higher expression in NHA-*CIC*^{KO} cells compared to NHA-*CIC*^{WT} cells in all phases (*ETV4*) or most phases (*ETV5*, except G2/M; Supplemental

Table S1; Benjamini-Hochberg [BH]-adjusted *p*-value < 0.1 and absolute fold-change > 1.5), supporting the validity of this approach.

In G2 and G2/M cells, several genes involved in the mitotic transition were differentially expressed between NHA-*CIC*^{WT} and NHA-*CIC*^{KO} cells (Supplemental Table S1), indicating that this process may be dysregulated in cells lacking functional CIC. Genes that showed lower expression in NHA-*CIC*^{KO} cells included positive regulators of the G2/M transition, such as *CCNB1* (Figure 1b), *CDK1* (Figure 1c), and members of the chaperonin containing TCP1 (CCT) complex (*CCT2*, *CCT4*, *CCT6A*, and *CCT8*; Supplemental Table S1). Conversely, several other genes involved in positive regulation of the G2/M transition were also found to be over-expressed in NHA-*CIC*^{KO} cells. These included *CDC25B* and *GTSE1* (Supplemental Figure S1b-c), which have both been implicated in G2/M checkpoint recovery and subsequent mitotic entry (Bugler et al. 2006; Jullien et al. 2011; Liu et al. 2010), as well as *BORA* (Supplemental Figure S1d), whose protein product functions with AURKA to activate PLK1, leading to CDK1 activation and mitotic entry (Seki et al. 2008). In M/G1 and G1/S cells, genes involved in G1 progression and the G1/S transition were also differentially expressed between NHA-*CIC*^{WT} and NHA-*CIC*^{KO} cells (Supplemental Table S1). For example, *CCNE2*, whose protein product functions with CDK2 to drive the G1/S transition (Abbas and Dutta 2009), had a lower abundance in NHA-*CIC*^{KO} G1/S cells (Figure 1d). Several genes encoding proteasomal subunits (*PSMA1*/*2*/*3*/*5*, *PSMB2*/*3*, *PSMC2*/*3*/*4*/*6*, *PSMD4*/*6*/*8*/*12*, *PSME2*, and *PSMG1*/*4*) and ubiquitin-conjugating enzymes (*UBE2A*, *UBE2D1*/*D2*/*D3*, *UBE2E1*/*E2*, *UBE2G1*, *UBE2L6*, *UBE2M*, *UBE2N*, and *UBE2V2*) were also less abundant in M/G1 and/or G1/S NHA-*CIC*^{KO} cells (Supplemental Table S1). Ubiquitination and subsequent proteasomal degradation of cell cycle regulatory proteins are important in mitotic progression, and downregulation of these processes could impair normal progression through mitosis (Bassermann et al. 2014). Together, these results indicate that the G2/M and G1/S transitions are likely dysregulated in CIC-deficient cells, potentially leading to abnormal accumulations of cells at several cell cycle stages as described above.

In addition to the dysregulation of genes involved in cell cycle transitions, we also found several genes associated with the spindle assembly checkpoint (SAC) and regulation of chromosomal alignment to be differentially expressed between NHA-*CIC*^{WT} and NHA-*CIC*^{KO} cells. For example, transcripts for the essential SAC components BUB3 and MAD2L1 were significantly less abundant in G2/M NHA-*CIC*^{KO} cells (Figure 1e-f). Notably, CCNB1 was also recently shown to function as an integral member of the SAC (Alfonso-Pérez et al. 2019; Hayward et al. 2019) and, as mentioned above, its transcript was also less abundant in mitotic NHA-*CIC*^{KO} cells. Genes involved in kinetochore and spindle function, which help ensure proper chromosome alignment, were also downregulated in G2/M NHA-*CIC*^{KO} cells. Examples include *CALM2*, *DYNC1LI1*, *NDC80*, *NPM1*, *SBDS*, *SEPTIN7*, *SPDL1*, and *ZWINT* (Supplemental Table S1). Both accurate SAC function and proper interactions between chromosomes and spindle microtubules are crucial to ensure error-free chromosome segregation, and defects in these processes have been shown to lead to chromosome segregation errors and aneuploidy (Gordon et al. 2012; Foley and Kapoor 2013). Therefore, dysregulated expression of genes involved in these processes in *CIC*^{KO} cells is compatible with the notion that such cells could be subject to defective mitosis. Our analyses thus showed that loss of CIC is associated with cell cycle stage-specific dysregulation of genes encoding critical mediators of error-free mitosis (e.g. SAC members) and fundamental regulators of cell cycle progression (e.g. *CDK1*, *CCNB1*, and *CDKN1A*).

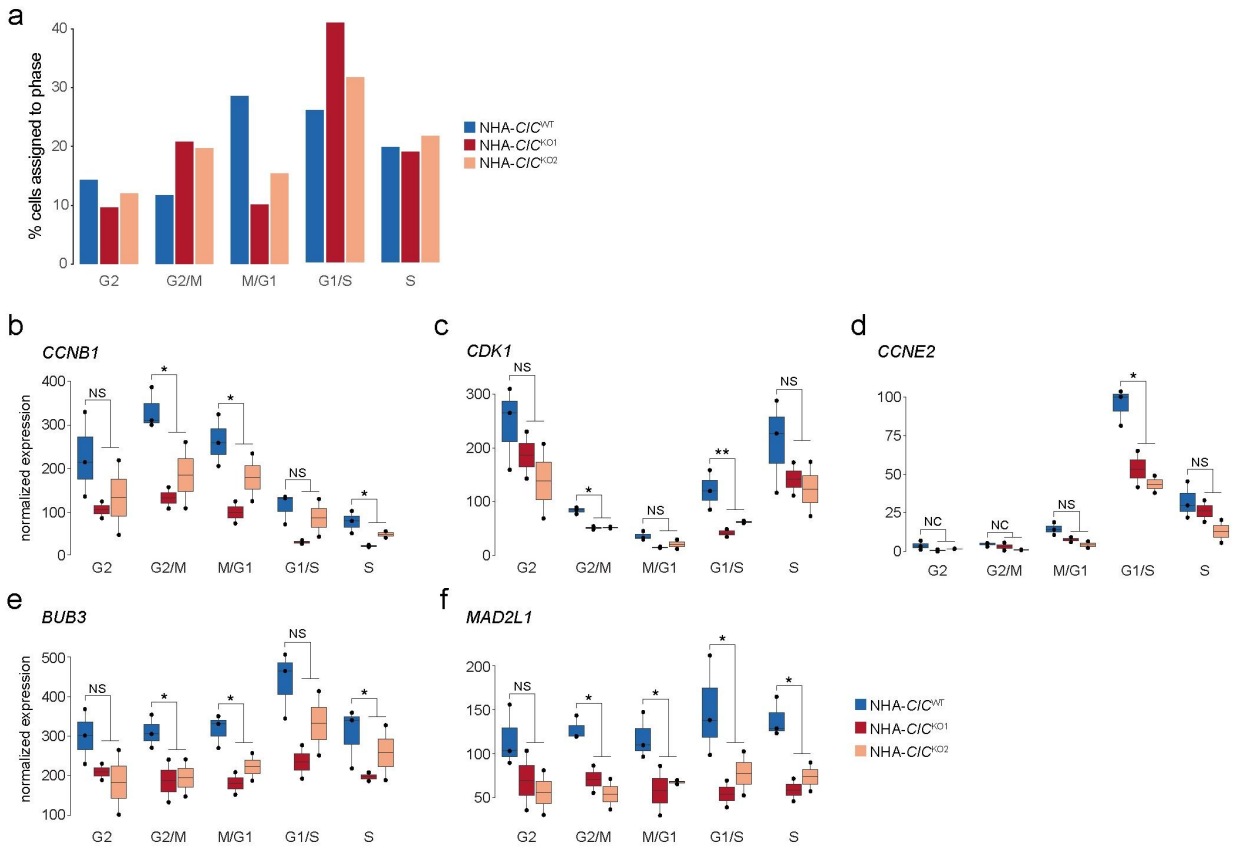

Figure 1: scRNA-seq analyses reveal differential expression of genes involved in cell cycle control between *CIC*^{WT} and *CIC*^{KO} cells.

a. Proportion of cells assigned to indicated cell cycle phase in each cell line (see Methods and Supplemental Figure S1a). **b-f.** Normalized expression of indicated genes across cell lines and phases. *BH-adjusted *p*-value < 0.1, ** < 0.01, *** < 0.001 (Wald test as implemented by DESeq2), NS: non-significant, NC: adjusted *p*-value not calculated due to low expression (Methods).

CIC is a transcriptional repressor of genes involved in cell cycle regulation

Given CIC's known function as a DNA-binding transcriptional repressor and the widespread dysregulation of mitotic regulators we observed in *CIC*^{KO} cells, we next sought to investigate whether CIC directly regulated the expression of cell cycle genes. To do this, we studied a set of 150 high-confidence CIC binding sites that our group previously identified in the NHA-*CIC*^{WT} line using chromatin immunoprecipitation followed by sequencing (ChIP-seq) (Lee et al. 2021). Of the 135 genes

associated with these binding sites (Supplemental Table S2), transcripts for 17 of them — *DUSP4*, *DUSP5*, *EPHA2*, *ETV4*, *ETV5*, *FAM118A*, *FOSL1*, *HMGA1*, *KMT5B*, *LINC0082*, *MAFF*, *OSGIN1*, *PDE4DIP*, *PLK3*, *PLPP4*, *TBC1D14*, and *TBC1D22A* — were differentially abundant between the parental NHA-*CIC*^{WT} cell line and at least one NHA-*CIC*^{KO} line in at least one cell cycle phase in our scRNA-seq data (Supplemental Table S1). The majority of these genes — except for *KMT5B*, *LINC0082*, and *PLPP4* — were more highly expressed in NHA-*CIC*^{KO} cells, which is consistent with CIC's known function as a transcriptional repressor. Given our previous observations that CIC loss was associated with dysregulated expression of cell cycle genes, we were particularly interested in *HMGA1* and *PLK3*, two genes that have previously been implicated in cell cycle regulation (Supplemental Figure S2). HMGA1, whose transcript was consistently overexpressed in NHA-*CIC*^{KO} cells (Figure 2a), has been shown to regulate the expression of multiple cell cycle genes, and its overexpression has oncogenic effects in various contexts (e.g. in models of breast cancer, cervical cancer, and lymphoid leukemia) (Vignali and Marracci 2020). *PLK3*, whose protein product is involved in regulating the G1/S transition (Zimmerman and Erikson 2007), was significantly more abundant in NHA-*CIC*^{KO1} cells in the G1/S phase and showed a trend towards higher expression in both NHA-*CIC*^{KO} lines at all phases (Figure 2b). Together, the overexpression of *HMGA1* and *PLK3* in NHA-*CIC*^{KO} cells and the observation that CIC binds to regulatory elements of these genes are consistent with the notion that these genes are targets of CIC transcriptional repression. Notably, the CIC ChIP peak identified near *PLK3* in NHA-*CIC*^{WT} cells overlaps with a CIC peak found in developing neuronal cells (Weissmann et al. 2018), indicating that CIC may bind to this region in different cellular contexts. Other cell cycle genes — specifically *CCND1*, *CDC14A*, *CDC14B*, and *MAFF* — also had evidence of overlapping proximal CIC binding sites in both our dataset and the Weissmann et al. (2018) dataset, indicating the possibility that these may also be targets of CIC-mediated transcriptional regulation (Supplemental Figure S2 and Supplemental Table S2).

To further evaluate *HMGA1* and *PLK3* as novel candidate targets of CIC transcriptional regulation, we performed additional CIC ChIP experiments followed by quantitative polymerase chain reaction (ChIP-qPCR) targeting the CIC peaks identified in the regulatory regions of these two genes. Previously validated CIC binding sites in the promoter regions of the known CIC target genes *ETV4* and *ETV5* were used as positive controls (LeBlanc et al. 2017) and showed significant enrichment in NHA-*CIC*^{WT} cells compared to NHA-*CIC*^{KO1} cells as expected (Figure 2c). The ChIP-seq-derived sites tested for *PLK3* and *HMGA1* also showed significant enrichment in NHA-*CIC*^{WT} cells compared to NHA-*CIC*^{KO1} cells (two-sided Student's *t*-test p-value < 0.05; Figure 2c), supporting CIC's role as a transcriptional regulator of these two genes. None of these sites, however, contained the known CIC binding motif (T[G/C]AATG[A/G]A) (Jimenez et al. 2012) even when allowing for up to two mismatches. Together, these results may indicate that: 1) CIC binds to a non-canonical motif within regulatory regions of *PLK3* and *HMGA1*, or 2) CIC functions as a co-repressor to regulate the expression of these genes and may rely on the DNA binding activity of other proteins to bind to these regions. Thus, these genes may be targeted by direct or indirect CIC binding.

To further confirm the observation that *HMGA1* and *PLK3* appear to be novel targets of CIC, we re-introduced CIC constructs into *CIC*^{KO} cells to determine whether the transcriptional repression of *HMGA1* and *PLK3* expression could be rescued. CIC exists in two isoforms — namely the long (CIC-L) and short (CIC-S) forms — and we have previously shown these to have different patterns of spatial distribution (Chittaranjan et al. 2014). We re-introduced each isoform (tagged with FLAG constructs) individually into the NHA-*CIC*^{KO1} cell line (NHA-*CIC*$^{KO1 + F\text{-}CIC\text{-}L}$ and NHA-*CIC*$^{KO1 + F\text{-}CIC\text{-}S}$, respectively; Figure 2d) and measured the expression of the candidate targets of interest and of the known CIC targets *ETV4* and *ETV5* using reverse transcription (RT)-qPCR. *ETV4* and *HMGA1* exhibited reduced expression upon re-introduction of either F-CIC-S or F-CIC-L, while *ETV5* and *PLK3* were re-repressed only upon re-introduction of F-CIC-S (two-sided Student's *t*-test p-value < 0.05, Figure 2e). Taken together, our

results support the hypothesis that CIC can regulate the expression of mitotic genes, and that *PLK3* and *HMGA1* are novel targets of CIC regulation. Furthermore, CIC's regulation of *PLK3* and *HMGA1* may occur through interaction with non-canonical CIC binding sites or through a co-repressor function involving other DNA-binding proteins.

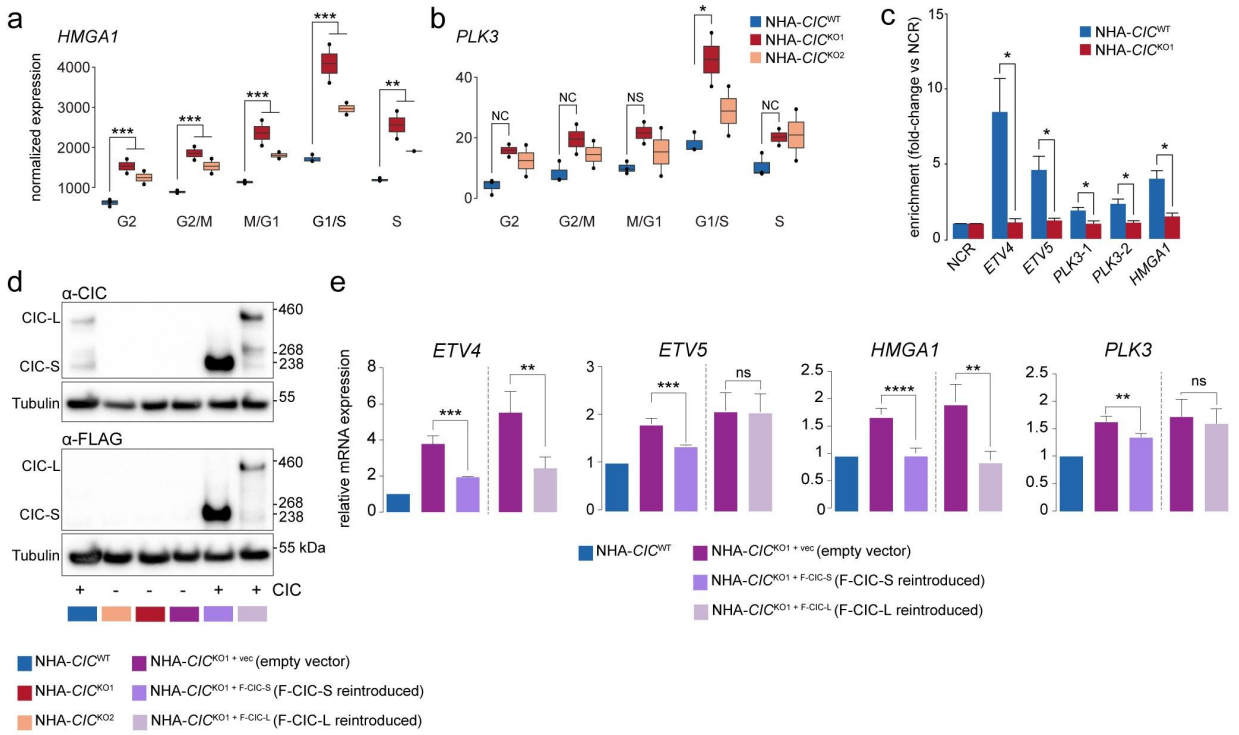

Figure 2. *HMGA1* and *PLK3* are targets of CIC-mediated transcriptional repression.

a-b. Normalized expression of indicated genes across cell lines and cell cycle phases. *adjusted *p*-value < 0.1, ** < 0.01, *** < 0.001 (Wald test as implemented by DESeq2), NS: non-significant, NC: adjusted *p*-value not calculated due to low expression (Methods). **c.** Enrichment of CIC binding at indicated sites relative to the negative control region (NCR), as measured using ChIP-qPCR against CIC. Bars represent the mean from three independent experiments, and error bars represent standard error of the mean (s.e.m.). **d.** Western blots showing expression of endogenous CIC (top) and FLAG-tagged CIC (bottom) in parental NHA-*CIC*^{WT} cells, NHA-*CIC*^{KO} cells, and NHA-*CIC*^{KO1} cells ectopically expressing either an empty vector, F-CIC-S, or F-CIC-L (detected using antibodies against CIC [top] or FLAG [bottom]). Tubulin is shown as a loading control. **e**. Expression of the known CIC targets *ETV4* and *ETV5* and of the putative novel targets *HMGA1* and *PLK3* in NHA-*CIC*^{KO1} cells expressing an empty vector or one of two CIC constructs (CIC-S or CIC-L), as measured by RT-qPCR. Expression is shown relative to the parental NHA-*CIC*^{WT} cells. Bars represent the mean of three independent experiments and error bars indicate s.e.m. **p*-value < 0.05, ** < 0.01, *** < 0.001, **** < 0.0001 (two-sided Student's *t*-test [c,e]).

Nuclear CIC interacts with mitotic regulators and SWI/SNF complex members

To further explore and refine the apparent link between CIC and cell cycle regulation, we next set out to characterize CIC's nuclear protein interaction network. We first performed immunoprecipitation (IP) assays for endogenous CIC and N-terminal MYC-fused CIC-S (using an anti-MYC antibody) in nuclear fractions purified from the HEK293A cell line (HEK-*CIC*^{WT}). The immunoprecipitates were then analyzed using liquid chromatography followed by tandem mass spectrometry (IP-MS; Methods). This yielded 291 candidate CIC-interacting proteins identified in at least two of the four IP-MS replicate experiments (Supplemental Table S3), including previously identified CIC protein interactors such as ATXN2L, SMARCA2, SMARCA4, SMARCC1, SMARCC2, and SVIL (Wong et al. 2019; Hwang et al. 2020). To identify pathways and protein complexes that were overrepresented in our list of candidate interactors, we performed enrichment analyses and identified mRNA splicing and metabolism, chromatin binding and organization, the G2/M checkpoint, transcription coregulator activity, and the CDC5L complex among the most significantly enriched processes and complexes (BH-adjusted p-value < 0.05; Supplemental Table S3; Methods). Given CIC's known function as a transcriptional regulator, the candidate interactors involved in transcription coregulation and chromatin structure reorganization were of particular interest. To determine whether these and other interactions could be replicated in the NHA context, we also performed IP-MS experiments using nuclear fractions of the NHA-*CIC*^{WT} cell line. Specifically, we performed a variation of the IP-MS technique in which 'trigger peptides' (Erickson et al. 2017) were used to enhance the sensitivity of the MS for a subset of proteins of interest (Figure 3a, Supplemental Table S4; Methods). This approach revealed candidate interactions between CIC and 456 proteins in the NHA context, 157 of which were observed in both the HEK and NHA lines (Supplemental Table S4; Methods). We considered these 157 proteins, which included the previously identified interactors ATXN1L, ATXN2L, SMARCA2, SMARCC1, and SMARCC2, to be high-confidence

candidate CIC interactors. Analysis of these 157 proteins once again yielded enrichment for RNA splicing, chromatin binding, the G2/M checkpoint, and the CDC5L complex (BH-adjusted p-value < 0.05; Supplemental Table S4; Methods), indicating that these functions are enriched in both cell lines.

As CIC is a transcriptional repressor and our data imply that CIC has a role in cell cycle gene expression regulation, we were particularly interested in high-confidence interactors involved in the G2/M checkpoint, the CDC5L complex, and chromatin binding and organization. The CDC5L complex is a pre-mRNA splicing factor and a regulator of mitotic progression (Mu et al. 2014), and several complex proteins — most notably CDC5L, a core complex component — were identified as high-confidence candidate interactors (Supplemental Table S4). Interestingly, the high-confidence candidate interactors also included NPM1, which is involved in cell cycle-associated functions such as centrosome licensing and G2/M checkpoint activation; is located at spindle poles during mitosis (Heath et al. 2017; Okuda et al. 2000); and which we found to be relatively under-expressed in CIC^{KO} cells (Supplemental Table S1). These observations are compatible with the notion that CIC may contribute to some aspect of chromosome separation through physical interactions with known mitotic factors, in addition to regulating transcripts of genes encoding such factors, as described above.

Among the high-confidence interactors associated with chromatin binding and organization, we identified several members of the SWI/SNF complex, including SMARCA2, SMARCC1, SMARCC2, and PBRM1. ARID1A and ARID2 were also identified as interactors in the NHA line, but not in HEK cells. Dysregulation of SWI/SNF complex members has been linked to mitotic defects (Coisy-Quivy et al. 2006; Dykhuizen et al. 2013; Brownlee et al. 2014; Xue et al. 2000). Given this link and the fact that CIC and the SWI/SNF complex were shown to cooperatively repress the expression of neuronal development genes (Hwang et al. 2020), we hypothesized that CIC's interaction with members of the SWI/SNF complex might be linked to a potential role in mitotic regulation. To first confirm these high-confidence interactions, we performed reciprocal IPs by immunoprecipitating SWI/SNF complex members and

probing with CIC, validating the interactions between endogenous CIC and SMARCA2, SMARCC1, ARID1A, and ARID2 in the NHA-*CIC*^{WT} line (Figure 3b-e), but not between CIC and PBRM1 (data not shown). We also performed immunofluorescence (IF) colocalization assays in HEK-*CIC*$^{KO2 + F\text{-}CIC\text{-}S}$ cells and observed a striking apparent colocalization between F-CIC-S and ARID1A, ARID2, SMARCA2, SMARCC1 (Figure 3f-g and Supplemental Figure S3a-b). Interestingly, we found that these proteins were dynamically re-distributed in the cell over the course of the cell cycle. SMARCA2, SMARCC1, and ARID1A showed apparent colocalization with and similar localization dynamics to CIC over the entire course of the cell cycle. Conversely, ARID2 appeared to surround decondensing chromosomes in late telophase and colocalized with CIC only later at early cytokinesis, when PBAF (a SWI/SNF complex containing ARID2 that has been observed to localize to kinetochores and spindle poles in mitotic cells (Xue et al. 2000)) is no longer localized to kinetochores. Although physical interactions between CIC and ARID1A and ARID2 were only identified in IP-MS experiments performed in NHA cells, as mentioned above, these results indicate the possibility that CIC may also interact, or at least colocalize, with these proteins in HEK cells. To further characterize these apparent colocalization patterns, we also performed proximity ligation assays (PLAs), which emit a fluorescent signal when antibodies targeting candidate protein interactors are within 40 nm of each other (Söderberg et al. 2006). In HEK-*CIC*$^{KO2 + F\text{-}CIC\text{-}S}$ cells, PLA signals were compatible with colocalization between F-CIC-S and ARID1A, SMARCA2, SMARCC1, and ARID2 during interphase (Figure 3h). Notably, the PLA signals were predominantly observed in the nucleus, indicating nuclear interactions. The most abundantly observed signal was for ARID1A, followed by SMARCA2, perhaps indicating that CIC interacts with these two proteins more frequently than the other SWI/SNF complex members we tested. Overall, these results appear to indicate spatial relationships between CIC and SWI/SNF complex proteins, and are compatible with the notion that CIC functions with the SWI/SNF complex, potentially in the context of mitotic regulation.

To further probe the intriguing patterns of CIC nuclear localization observed above, we performed IF assays in the NHA-*CIC*^{WT} line and a human oligodendroglioma (HOG) line (HOG-*CIC*^{WT}) (Post and Dawson 1992) (Figure 3i, Supplemental Figure S3c). Endogenous CIC was observed throughout nuclei during interphase, but appeared to be excluded from condensed chromosomes at metaphase and telophase. During early cytokinesis, CIC foci appeared at de-condensing chromosomes during initiation of nuclear envelope reassembly, and increasingly accumulated until completion of cytokinesis. Upon completion of nuclear envelope assembly, CIC was once again observed throughout the nucleus. We also confirmed this observation in HEK-*CIC*$^{KO2 + F\text{-}CIC\text{-}S}$ cells, where ectopically expressed F-CIC-S displayed similar localization dynamics as endogenous CIC (Supplemental Figure S3d). To determine if CIC's distinct dynamic localization pattern was consistent with a structural role, we performed IF colocalization assays using markers of key mitotic structures, namely α-tubulin, CENPA, and AURKB, to observe spindles, centromeres, and the midbody, respectively (Supplemental Figure S3e-g). CIC did not appear to be associated with spindle structures, centromeres and kinetochore attachments, or the midbody over the course of the cell cycle, indicating that it is unlikely to play a structural role in ensuring proper mitotic segregation. Thus, CIC's dynamic re-localization over the course of mitosis may be related to CIC's apparent role in cell cycle regulation, although this role does not appear to be structural in nature.

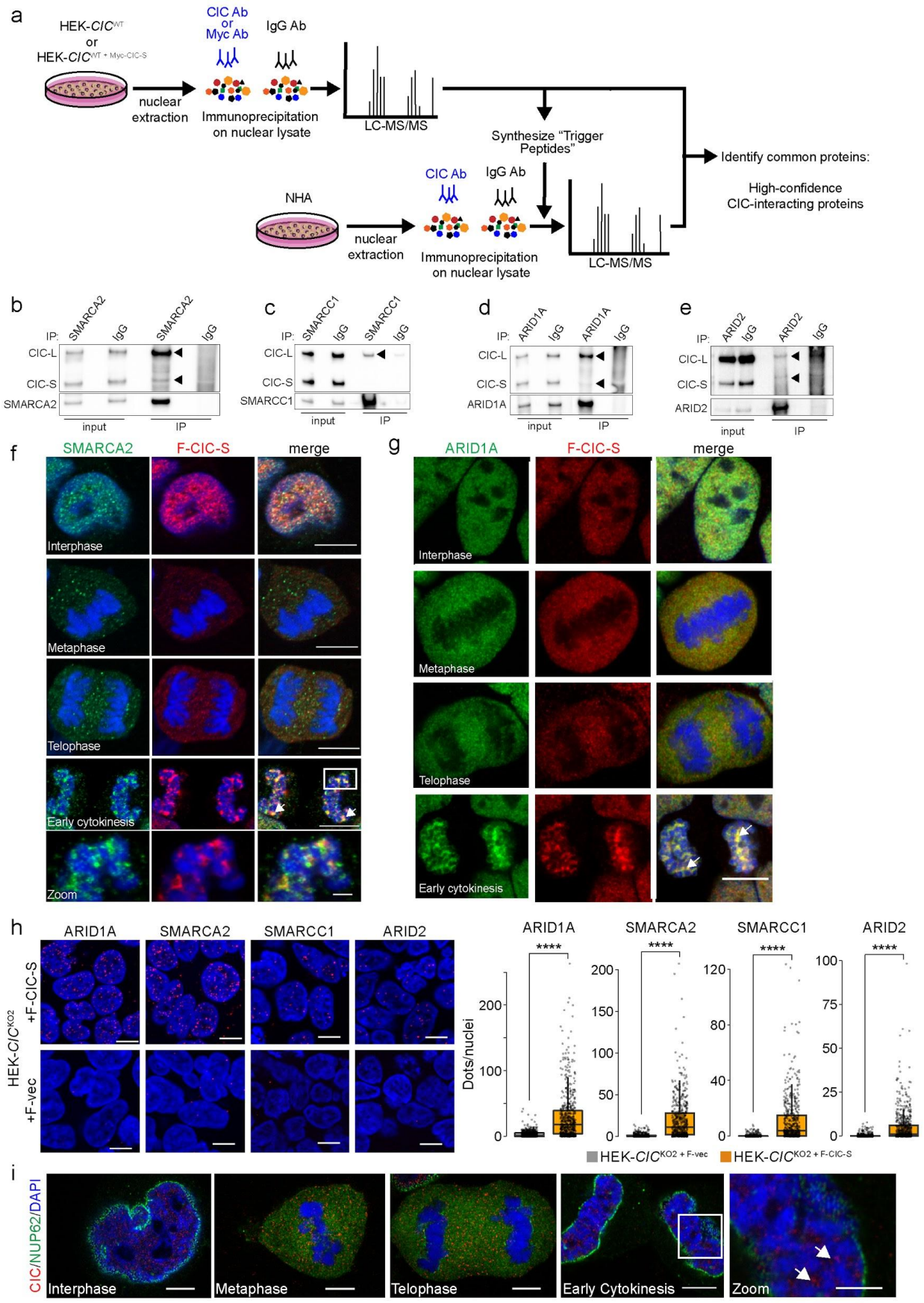
a
HEK-CIC^WT
or
HEK-CIC^WT + Myc-CIC-S
nuclear extraction
CIC Ab or Myc Ab
IgG Ab
Immunoprecipitation on nuclear lysate
LC-MS/MS
Synthesize "Trigger Peptides"
NHA
nuclear extraction
CIC Ab
IgG Ab
Immunoprecipitation on nuclear lysate
LC-MS/MS
Identify common proteins:
High-confidence CIC-interacting proteins
b
IP: SMARCA2 IgG SMARCA2 IgG
CIC-L
CIC-S
SMARCA2
input IP
c
IP: SMARCC1 IgG SMARCC1 IgG
CIC-L
CIC-S
SMARCC1
input IP
d
IP: ARID1A IgG ARID1A IgG
CIC-L
CIC-S
ARID1A
input IP
e
IP: ARID2 IgG ARID2 IgG
CIC-L
CIC-S
ARID2
input IP
f
SMARCA2 F-CIC-S merge
Interphase
Metaphase
Telophase
Early cytokinesis
Zoom
g
ARID1A F-CIC-S merge
Interphase
Metaphase
Telophase
Early cytokinesis
h
ARID1A SMARCA2 SMARCC1 ARID2
HEK-CIC^KO2
+F-CIC-S
+F-vec
ARID1A SMARCA2 SMARCC1 ARID2
****
Dots/nuclei
HEK-CIC^KO2 + F-vec
HEK-CIC^KO2 + F-CIC-S
i
CIC/NUP62/DAPI
Interphase
Metaphase
Telophase
Early Cytokinesis
Zoom

Figure 3. CIC interacts with members of the SWI/SNF complex.
a. Workflow of CIC IP-MS in HEK-*CIC*^{WT} and NHA-*CIC*^{WT} cell lines. See Methods section for more detail. **b-e**. Reciprocal IPs confirming interactions between CIC and select SWI/SNF subunits. SMARCA2 (b), SMARCC1 (c), ARID1A (d), and ARID2 (e) were immunoprecipitated from nuclear lysates of the parental NHA-*CIC*^{WT} cell line, and CIC interaction was visualized by western blot. Input lanes indicate nuclear lysate samples used as input for the respective IPs. CIC-L and CIC-S bands are marked with arrowheads. **f-g**. Localization of F-CIC-S (FLAG, red), SMARCA2 (f, green), and ARID1A (g, green) in HEK-*CIC*$^{KO2 + F\text{-}CIC\text{-}S}$ cells at indicated phases of the cell cycle, detected by IF. DNA was stained with DAPI (blue). Arrows indicate colocalization of CIC and the relevant interactor at early cytokinesis (yellow foci). Scale bars: 10 µm and 5 µm (zoomed image in f). **h**. Left: representative PLAs using antibodies against FLAG and ARID1A, SMARCA2, SMARCC1, or ARID2 in HEK-*CIC*^{KO2} cells expressing F-CIC-S (HEK-*CIC*$^{KO2 + F\text{-}CIC\text{-}S}$, top) or an empty vector (HEK-*CIC*$^{KO2 + F\text{-}Vec}$, bottom). DNA was visualized using DAPI staining (blue), and PLA spots indicating proximity of the proteins assayed (< 40 nm) are visualized in red. Right: Tukey boxplots showing quantifications of PLA spots per nuclear region. ARID1A, n = 732 and 583; SMARCA2, n = 564 and 533; SMARCC1, n = 564 and 533; ARID2, n = 564 and 588 (nuclei counts for HEK-*CIC*$^{KO2 + F\text{-}Vec}$ and HEK-*CIC*$^{KO2 + F\text{-}CIC\text{-}S}$, respectively). ****$p$-value < 0.0001 (Welch's t-test). **i**. IF staining of endogenous CIC (red) and the nuclear envelope protein NUP62 (green) in the parental NHA-*CIC*^{WT} line. CIC shows a punctate localization pattern (arrows) throughout the decondensing nucleus. Scale bars: 10 µm and 5 µm (zoomed image).

CIC shares essentiality and genetic interactions with genes involved in cell cycle and mitotic regulation

Genes that encode proteins that function in similar biological pathways often exhibit similar fitness patterns when perturbed in genetic screens, and mapping these coordinated fitness effects (or "co-essentialities") can be used to group genes into related pathways and identify novel gene functions (Michel et al. 2018; Pan et al. 2018). To identify genes that exhibited co-essentialities with *CIC*, we leveraged fitness effect scores that were calculated from genome-wide KO screens performed by the Cancer Dependency Map (DepMap) project (Meyers et al. 2017; Dempster et al. 2019; DepMap 2020). Briefly, DepMap researchers used CRISPR-Cas9-based screening experiments to knock out a single gene per cell, allowing for measurement of the effect of a single gene loss on cell viability (Meyers et al. 2017). This measure is called the fitness effect score. We calculated Pearson coefficients between fitness effect scores of *CIC* and 18,332 genes that were perturbed in 739 cancer cell lines, and found 88 genes that were co-essential with *CIC* (Pearson coefficient > 0.178 and BH-adjusted p-value < 0.05; Figure 4a; Supplemental Table S5; Methods). Among these genes was *ATXN1L*, which encodes a protein known to

interact with and stabilize CIC for DNA binding (Wong et al. 2019), as well as *DUSP6*, a known target of CIC repression (LeBlanc et al. 2017). Notably, the highest correlation — besides *CIC* with itself — was observed between *CIC* and *ERF* perturbations (Pearson coefficient = 0.30 and BH-adjusted *p*-value = 3.07×10^{-13}). Similar to CIC, ERF is an ETS domain transcriptional repressor and an ERK-dependent kinase that functions as an effector of the receptor tyrosine kinase (RTK) signaling pathway (Le Gallic et al. 2004). ERF has also been shown to regulate the cell cycle, and loss of ERF activity can lead to G1 arrest (Le Gallic et al. 2004). Our analysis also identified *BICRA* (Pearson coefficient = 0.20 and BH-adjusted *p*-value = 1.55×10^{-8}), a gene that encodes the SWI/SNF complex member GLTSCR1. GLTSCR1 has only recently been identified as a member of the GBAF SWI/SNF complex (Alpsoy and Dykhuizen 2018), and thus GLTSCR1's role as a SWI/SNF subunit is not fully understood. Notably, knockdown of another GBAF subunit member, SMARCA4, was shown to reduce cell proliferation and induce cell cycle arrest (Innis and Cabot 2020; Giles et al. 2021), a role that may be shared by other GBAF members. Within the 88 co-essential genes, we found a significant enrichment for genes with functions related to regulation of attachment of spindle microtubules to kinetochores (*BECN1* and *SIRT2*; BH-adjusted *p*-value = 0.0015) and regulation of exit from mitosis (*TGFB1* and *SIRT2*; BH-adjusted *p*-value = 0.0031; Figure 4b; Supplemental Table S5; Methods). *CIC*'s co-essentiality network thus indicates coordinated fitness effects with cell cycle and mitotic regulators, which is consistent with our data implying that CIC may play a role in these processes.

We further leveraged DepMap data (Meyers et al. 2017; Dempster et al. 2019; Ghandi et al. 2019; Nusinow et al. 2020; DepMap 2020) to perform *in silico* genome-wide genetic perturbation screens to identify genes that might genetically interact with *CIC*. We screened for genetic alterations that, in *CIC* mutant cells, resulted in decreases or increases of cell viability relative to CIC^{WT} control cell lines (Supplemental Figure S4a; Methods). Such genetic screening approaches can reveal interactions between

genes that encode proteins that do not necessarily interact physically, such as synthetic lethal (SL) and alleviating genetic interactions (Nijman 2011; van Leeuwen et al. 2017).

Using genome sequencing data from DepMap (Ghandi et al. 2019), we identified a non-small cell lung cancer line (HCC-366) and an endometrial carcinoma line (JHUEM1) with homozygous deleterious alterations predicted to abrogate CIC function (*CIC*^{HomDel}; Supplemental Figure S4b; Supplemental Table S6; Methods). Notably, the mutation in JHUEM1 is exclusive to the CIC-L isoform (Supplemental Figure S4b); therefore, JHUEM1 may retain at least some CIC activity through the CIC-S isoform. We also identified five cancer cell lines with deleterious potentially *trans*-heterozygous *CIC* mutations (i.e. two or more mutations, all in regions common to the CIC-S and CIC-L isoforms; *CIC*$^{\text{T-HetDel}}$), 53 lines with heterozygous deleterious *CIC* mutations (six of which were exclusive to the CIC-L isoform; *CIC*^{HetDel}), and 557 *CIC*^{WT} lines (Supplemental Table S6; Methods). To infer the presence of functional CIC in these different cell lines, we used DepMap transcriptome and proteome data (Ghandi et al. 2019; Nusinow et al. 2020) to investigate mRNA and protein abundance of *CIC* and *ETV4*/*5* (known targets of CIC transcriptional repression). Compared to *CIC*^{WT} lines, we observed a significant decrease in *CIC* mRNA levels only in *CIC*^{HetDel} lines (analysis of variance [ANOVA] p-value = 0.0041, Tukey's Honest Significant Difference [HSD] test p-value < 0.01; Figure 4c), indicating that the aberrant forms of *CIC* in *CIC*$^{\text{T-HetDel}}$ and *CIC*^{HomDel} lines encoded wild type levels of *CIC* transcripts (Tukey's HSD > 0.05). In contrast, we observed a significant decrease in CIC protein levels in *CIC*^{HetDel} and *CIC*$^{\text{T-HetDel}}$ lines compared to *CIC*^{WT} lines (ANOVA p-value = 0.0021, Tukey's HSD test p-value < 0.01 and < 0.05, respectively; Figure 4c). Protein data were not available in DepMap for the *CIC*^{HomDel} lines. *CIC*^{HomDel} and *CIC*$^{\text{T-HetDel}}$ cell lines both displayed trends towards higher mRNA expression of *ETV4* and *ETV5* compared to *CIC*^{WT} lines (ANOVA p-value > 0.05; Supplemental Figure S4c; Methods). Given the reduced CIC protein expression observed in *CIC*$^{\text{T-HetDel}}$ and *CIC*^{HetDel} lines and the moderate increases in *ETV4* and *ETV5* mRNA levels observed in

CIC$^{\text{T-HetDel}}$ and *CIC*^{HomDel} lines, we deduced that the *CIC*^{HomDel} and *CIC*$^{\text{T-HetDel}}$ cell lines likely lack, or have reduced, CIC activity and were therefore good candidates to use for *in silico* genetic screening analyses.

We first conducted an *in silico* genome-wide screen by comparing the lethality outcomes of gene KOs in *CIC*^{HomDel} lines and *CIC*^{WT} lines across 18,322 genes (Methods). Briefly, we made use of a CRISPR-Cas9 KO screen-derived measure called the "lethality probability", which normalizes the fitness effect scores to account for variability in screen quality between cell lines and is provided with DepMap data (Meyers et al. 2017; Dempster et al. 2019). This measure is scaled from 0 to 1, where a probability of 0 indicates a non-essential gene (i.e. the gene KO did not affect cell viability) and a probability of 1 indicates an essential gene that was necessary for the survival of that cell line (Meyers et al. 2017; Dempster et al. 2019). Genes that had significantly different lethality probabilities between *CIC*^{HomDel} and *CIC*^{WT} cell lines (defined as having an absolute $\log_2$ fold-change of median lethality probabilities > 1.5, a Mann-Whitney U test p-value < 0.05, and a median lethality probability > 0.5 in at least one group; Methods) were defined as candidate genetic interactors of *CIC*. We identified 48 such genes, all of which were predicted to be SL interactors of *CIC* (i.e. had significantly higher lethality probabilities in *CIC*^{HomDel} lines than in *CIC*^{WT} lines; Figure 4d, Supplemental Table S7). An enrichment analysis (Methods) to identify functional patterns associated with SL interactors did not reveal statistically significant terms after multiple testing correction (Supplemental Table S7). However, SL interactors did show a trend towards the enrichment of the terms "M phase" (R-HSA-68886) and "mitotic cell cycle process" (GO:1903047; uncorrected p-values = 0.0043 and 0.0057, respectively; Supplemental Table S7). Given our other observations that mitotic genes appeared dysregulated in cells lacking CIC and that SL interactors showed a trend towards enrichment of cell cycle processes, we focused on genes that were associated with these mitotic and cell cycle-associated terms, namely *ANKRD17*, *BECN1, CDK10*, *CKAP2*, *CSNK2A1*, *HAUS2*, *LEMD2*, and *UBE2S* (Supplemental Table S7). *CSNK2A1* and *UBE2S*, in particular, encode proteins that are involved in the SAC and the anaphase-promoting complex (APC/C)

(St-Denis and Litchfield 2009; Bremm and Komander 2011). BECN1 promotes accurate kinetochore anchoring to mitotic spindles and proper cytokinetic abscission (Frémont et al. 2013; You et al. 2016) and, notably, we also identified *BECN1* as being co-essential with *CIC*, as described above (Figure 4a, Supplemental Table S5). The identification of *BECN1* as both co-essential with and a SL interactor of *CIC* indicates that CIC likely plays a synergistic role either serially or in parallel with BECN1, and that inactivation of these two genes together may not be compatible with cell survival.

To determine whether $CIC^{\text{T-HetDel}}$ cell lines showed genetic interactions that were similar to those that were identified in CIC^{HomDel} cell lines, we conducted another *in silico* screen comparing $CIC^{\text{T-HetDel}}$ and CIC^{WT} cell lines. We identified 58 candidate interactors that were predicted as SL (n = 48) or alleviating interactors (n = 10) of *CIC* (Mann-Whitney U test p-value < 0.05 and a median lethality probability > 0.3 in at least one group; Supplemental Table S8; Methods). These candidate genes did not overlap with interactors identified using CIC^{HomDel} cell lines. However, we again observed a trend towards the enrichment of the "mitotic cell cycle process" term that we saw using CIC^{HomDel} lines, as described above (GO:1903047; uncorrected p-value = 9.09×10^{-4} for the $CIC^{\text{T-HetDel}}$ interactors; Supplemental Table S8; Methods). Similarly to the enrichment analysis of candidate interactors identified using CIC^{HomDel} cell lines, no terms were found to be significantly enriched following multiple testing correction; however, we did observe trending enrichments in other related mitotic terms — such as "cytoplasmic microtubule", "regulation of cytoskeleton organization", and "spindle pole" (Supplemental Table S8) — and these terms included both SL and alleviating candidate interactors. Together, the consistent enrichment of candidate genetic interactors that are associated with mitotic processes observed in both CIC^{HomDel} and $CIC^{\text{T-HetDel}}$ cell lines implies that *CIC* genetically interacts with mitotic regulators across cancer cell lines.

Interestingly, the predicted SL interactors identified in CIC^{HomDel} cell lines included *ARID2*, a SWI/SNF family member that we also identified as a physical interactor of CIC in NHA cells using IP-MS. The lethality probabilities of *ARID2* KO in the two CIC^{HomDel} cancer cell lines were 0.891 and

0.980 (compared to a median probability of 0.296 in the *CIC*^{WT} cell lines), which is compatible with the notion that ARID2 is necessary for the survival of these *CIC*^{HomDel} cancer cell lines. This interaction is particularly striking since PBAF, a SWI/SNF complex containing ARID2, has previously been observed to localize to kinetochores and spindle poles in mitotic cells (Xue et al. 2000). The predicted SL interaction between *CIC* and *ARID2* is thus consistent with a potential role for a *CIC* - *ARID2* interaction in mitosis. Although the cell cycle-related genetic interaction partners identified in this analysis regulate several different cell cycle and mitotic functions, when considered together, they may indicate CIC's involvement in cell cycle processes and a vulnerability of cells lacking CIC to further cell cycle and/or mitotic dysregulation.

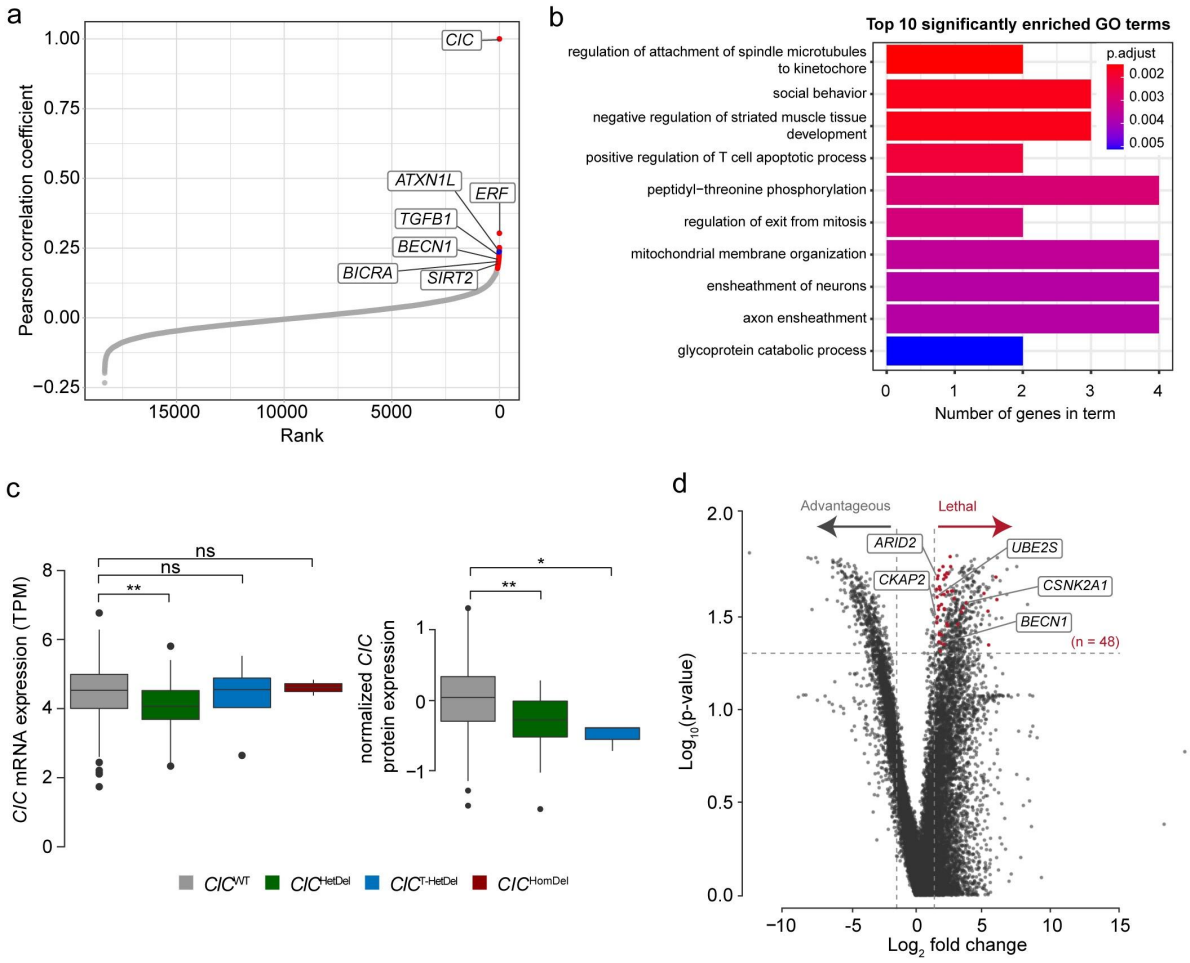

Figure 4. *CIC* is predicted to share co-essentialities and synthetic lethal interactions with mitotic regulators.

a. Pearson correlation coefficients between the lethality probabilities of *CIC* and those of all genes targeted by DepMap genetic screens (n = 18,332) across 739 cancer cell lines. Red points indicate genes with coefficients above the inflection point (88 genes; coefficient > 0.178). The blue point indicates the coefficient of *ATXN1L*. **b.** Top ten GO biological processes enriched for genes that are co-essential with *CIC* (red points in panel a). **c.** Transcriptomic and proteomic data from DepMap were compared across cancer cell lines. Left: *CIC* mRNA abundance in CIC^{HomDel} (n = 2), $CIC^{\text{T-HetDel}}$ (n = 5), CIC^{HetDel} (n = 53), and CIC^{WT} (n = 557) cancer cell lines. mRNA expression values were normalized to transcripts per million (TPM). ANOVA *p*-value = 0.00407. Right: protein expression in $CIC^{\text{T-HetDel}}$ (n = 3), CIC^{HetDel} (n = 16), and CIC^{WT} (n = 189) cancer cell lines. CIC protein expression values were normalized and mean-centered (see Methods). ANOVA (*p*-value = 0.00217) followed by Tukey's HSD analysis. **p*-value < 0.05, ** < 0.01. **d.** Volcano plot of differentially lethal genes. Each point represents the differential lethality effect of a single gene KO compared between CIC^{HomDel} and CIC^{WT} cancer cell lines. Red points indicate significant genetic interactors (Mann-Whitney U test *p*-value < 0.05, absolute $\log_2$ fold-change > 1.5, and median lethality probability > 0.5 in at least one cell line group; Methods).

Loss of CIC is associated with mitotic defects in mammalian cells

Given the dysregulated expression of mitotic genes in *CIC*^{KO} cells and CIC's proteomic and genetic interactions with mitotic regulators, we next asked whether loss of CIC would result in an aberrant mitotic phenotype in cells. Using IF assays, we observed that NHA-*CIC*^{KO} lines had an increased frequency of mitotic defects compared to the parental NHA-*CIC*^{WT} cells. Specifically, the *CIC*^{KO} lines (NHA-*CIC*^{KO1} and NHA-*CIC*^{KO2}) showed 2.2 - 2.5-fold increases in metaphase alignment defects (two-sided Student's *t*-test p-value < 0.05) and 2 - 2.3-fold increases in chromosome segregation defects (e.g. lagging chromosomes and micronuclei) at telophase/cytokinesis (p-value < 0.01; Figure 5a-b). We also observed a significant increase in metaphase defects in HEK-*CIC*^{KO} cell lines compared to HEK-*CIC*^{WT} cell lines (Supplemental Figure S5), indicating that the association between CIC loss and increased frequency of mitotic defects is not specific to the NHA-derived lines.

To determine if this phenotype extended beyond mammalian cell lines, we performed additional IF assays in brain sections from E13.5 mice with forebrain-specific *Cic* loss (*Cic*$^{fl/fl}$; *FoxG1*$^{cre/+}$) and from heterozygous control mice (*Cic*$^{fl/+}$; *FoxG1*$^{cre/+}$) (Ahmad et al. 2019). Consistent with our *in vitro* results, *Cic*-null cells in the mitotically active ventricular zone displayed an increased frequency of mitotic defects, including lagging chromosomes and micronuclei (average 2.5-fold increase, two-sided Student's *t*-test p-value < 0.0001; Figure 5c). Together, these observations indicate a previously unappreciated relationship between CIC loss and mitotic defects in mammalian cells *in vitro* and *in vivo*.

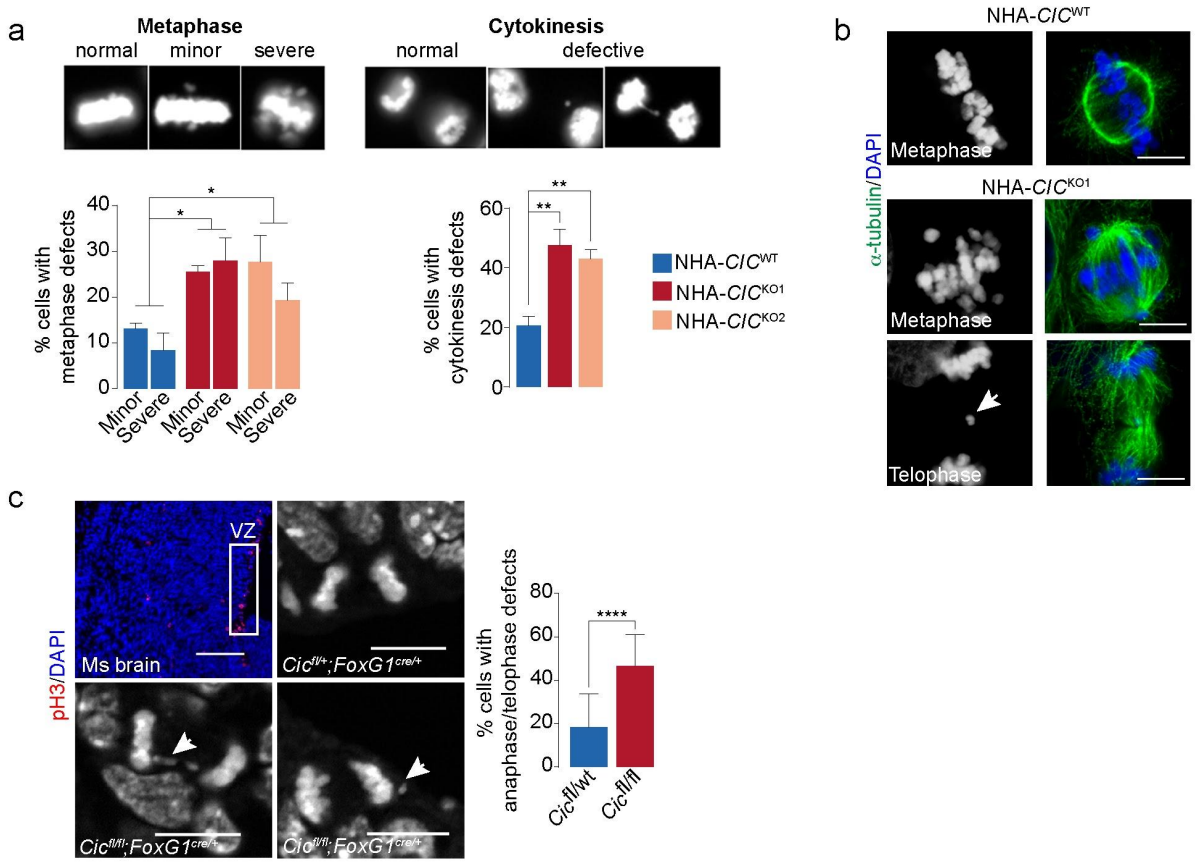

Figure 5: Cells lacking CIC have an increased frequency of mitotic defects.

a. Top: representative images of NHA cells with normal or defective metaphase and cytokinesis. Bottom: proportions of cells from indicated cell lines assigned to each category. Bars represent the mean from three independent experiments and error bars indicate s.e.m. NHA-*CIC*^{WT}, n = 146 and 122; NHA-*CIC*^{KO1}, n = 99 and 94; NHA-*CIC*^{KO2}, n = 104 and 89 (metaphase and cytokinesis cell counts, respectively). **b**. Representative images of an NHA-*CIC*^{WT} cell with normal metaphase (top) and NHA-*CIC*^{KO1} cells with defective metaphase alignment (middle) and a lagging chromosome at telophase (arrowhead, bottom). Left: DAPI staining alone. Scale bars: 10 µm. **c**. Left: mitotically active (boxed) ventricular zone (VZ) region from an E13.5 Cic$^{fl/+}$;FoxG1$^{cre/+}$ mouse forebrain and representative images of a normal cell division in a *Cic*$^{fl/+}$;*FoxG1*$^{cre/+}$ mouse (top right) and a lagging chromosome and a micronucleus in *Cic*$^{fl/fl}$;*FoxG1*$^{cre/+}$ mice (arrowheads, bottom left and right, respectively). Right: proportions of cells with defective anaphase/telophase. Bars represent the mean from four animals for each genotype and error bars indicate s.e.m (n = 186 cells for *Cic*$^{fl/+}$;*FoxG1*$^{cre/+}$ mice and 180 for *Cic*$^{fl/fl}$;*FoxG1*$^{cre/+}$ mice). Scale bars: 100 µm (top left) and 10 µm. **p*-value < 0.05, ** < 0.01, **** < 0.0001 (two-sided Student's *t*-test [a,c]).

Discussion

In this study, we used a multi-omics approach to probe CIC's role in transcriptional regulation and map its proteomic and genetic interactomes in human cells, with results from those orthogonal approaches appearing to converge onto a novel role for mammalian CIC in regulating mitotic fidelity and cell cycle progression. Using a scRNA-seq approach, we were able to survey the transcriptional consequences of CIC loss at different stages of the cell cycle, and observed dysregulated expression of key mitotic and cell cycle progression genes within cycling cells. Mapping of CIC's proteomic and genetic interaction networks further supported a mitotic role, with physical CIC interactors, predicted genetic interactors, and *CIC*'s co-essential genes showing functional enrichment of processes including mitotic-specific cytoskeleton organization, kinetochore function, centrosome organization, and mitotic entry and exit regulation. For example, *BECN1*, which was predicted to share co-essentiality and lethal genetic interactions with *CIC*, encodes a protein that localizes on microtubules and near the outer kinetochores and regulates proper attachment of mitotic microtubules to kinetochores during mitosis (Frémont et al. 2013; You et al. 2016). Our results indicate that CIC may share similar roles in supporting the formation of mitotic structures, or may be involved in a parallel role that converges with BECN1's function in maintaining mitotic fidelity, which is essential for cell survival. Although the inhibition of *BECN1* expression leads to phenotypes similar to the ones we observed in CIC-deficient cells, such as an increased frequency of cytokinesis defects (Frémont et al. 2013), we did not observe colocalization between CIC and spindle structures or centromeres and kinetochore attachments over the course of the cell cycle. Therefore, CIC may function in parallel with BECN1 through a non-structural role. Dysregulation of other genes that our results indicated were transcriptionally regulated by CIC (e.g. *MAD2L1* and *BUB3* (Foijer et al. 2017; Warren et al. 2002; Kalitsis et al. 2000)) or that were predicted to be SL interactors with *CIC* (e.g. *CKAP2* (Hong et al. 2009b; Yoo et al. 2017)) has also previously been shown to result in chromosomal misalignment and missegregation. Their possible disruption due to CIC

loss could thus contribute to the phenotypes we observed in *CIC*^{KO} cells, such as increased incidence of lagging chromosomes and nuclei, which are phenotypes reminiscent of those observed in cells with dysregulated SAC function (Zhang et al. 2015; Ricke et al. 2011). Together, these results reinforce the notion that CIC functions to regulate mitotic progression and chromosome segregation, and that loss of CIC leads to errors in these processes.

Our mapping of CIC's proteomic and genetic interaction networks in cell lines also revealed interactions between CIC and members of the chromatin-modifying SWI/SNF complex. A recent study showed that CIC interacts with SWI/SNF complex members to influence neuronal development, and that this interaction is necessary for the proper regulation of genes involved in this process (Hwang et al. 2020). Our IP-MS results support and extend these observations, revealing cell cycle-specific physical interactions between CIC and ARID1A, ARID2, SMARCA2, SMARCC1, and SMARCC2 in human cells. We found that CIC co-localized with ARID1A, SMARCA2, and SMARCC1 throughout the cell cycle, displaying a dynamic relocalization pattern that included foci formation at de-condensing chromosomes during initiation of nuclear envelope reassembly and accumulation of these foci until completion of cytokinesis. *CIC*'s co-essentiality analysis further revealed that CIC may share a functional role with the recently identified SWI/SNF member GLTSCR1, and our *in silico* genome-wide screen revealed a SL genetic interaction between *CIC* and *ARID2*. The SWI/SNF complex has been implicated in the maintenance of genomic stability, and disruption of its activity has been associated with mitotic defects similar to the ones we observed in this study (e.g. faulty chromosome segregation) (Coisy-Quivy et al. 2006; Dykhuizen et al. 2013; Brownlee et al. 2014; Xue et al. 2000). Our results thus indicate the possibility that CIC and the SWI/SNF complex function together to regulate cell cycle processes and promote mitotic fidelity, possibly through co-regulation of cell cycle genes.

Overall, our study considerably expands our knowledge of CIC's protein and genetic interactomes and presents evidence that CIC regulates the expression of cell cycle genes. We showed that CIC

displayed a dynamic relocalization pattern over the course of the cell cycle together with members of the SWI/SNF complex, and that loss of CIC was associated with an increased frequency of mitotic defects in human cell lines and a mouse model. The novel roles ascribed to CIC in this study thus cast it as a regulator of the cell cycle and mitotic stability in mammalian cells and may explain its function as an apparent tumor suppressor.

Methods

Cell culture

The IDH1-stable NHA cell line was obtained from Applied Biological Materials (ABM) Inc (T3022; Richmond, BC, Canada). The HEK293A cell line was obtained from Dr. Gregg Morin (Canada's Michael Smith Genome Sciences Centre, Vancouver, BC, Canada) and authenticated by Genetica DNA Laboratories (Cincinnati, OH, USA). The HOG cell line was obtained from Dr. G. Dawson (The University of Chicago, IL, USA). Cells were cultured in Dulbecco's Modified Eagle Medium (DMEM) supplemented with 10% (v/v) heat-inactivated (HI) FBS (Thermo Fisher Scientific, Waltham, MA, USA). Stable cell lines expressing F-CIC-S, F-CIC-L, or F-vec were cultured in DMEM + 10% HI FBS with Zeocin (Thermo Fisher Scientific) selection. Cell culture was performed in a humidified, 37°C, 5% CO_2 incubator.

CIC knockout cell line generation and expression constructs

CRISPR-Cas9 sgRNA sequences were designed to target exon 2 of the *CIC* gene, and *CIC*^{KO} lines were established from NHA (NHA-*CIC*^{KO1} [A2] and NHA-*CIC*^{KO2} [H9]) and HEK293A (HEK-*CIC*^{KO1} [A9] and HEK-*CIC*^{KO2} [D10]) cells as described previously (LeBlanc et al. 2017). *CIC* knockout status was verified by western blot and Sanger sequencing. N-terminal FLAG-CIC-short form (FLAG-CIC-S) and long-form (FLAG-CIC-L) plasmids were prepared as described previously (Chittaranjan et al. 2014).

scRNA-seq

Single-cell 3' RNA-seq libraries were generated using the Chromium Single Cell 3′ Library & Gel Bead Kit v1 (10X Genomics, Pleasanton CA) following the manufacturer's protocol. Full details can be found in the Supplemental Methods.

The CellRanger software was used to create fastq files (cellranger mkfastq with default parameters; v1.2.1) and to perform alignment, filtering, barcode counting, and UMI counting (cellranger count with default parameters except --expect-cells set to 1000 for all samples; v2.1.1). The CellRanger hg19-3.0.0 reference was used for alignment. Data preprocessing was performed in the R statistical software (v3.5.0) (R Core Team 2020), based on the filtered count matrices output by CellRanger. Counts for cells from all samples (7,735 cells) were combined into a single count matrix, and genes detected (UMI > 0) in at least two cells were retained. Normalization was then applied to all cells using the scran R package (Lun et al. 2016) (v1.10.1). The *quickCluster* function was used to cluster cells for normalization (with min.mean = 0.1 as suggested for UMI data), and the resulting clusters were used as input to the *computeSumFactors* function (with min.mean = 0.1). These factors were then used in the *normalize* function of the scater R package (v1.10.0).

Cells were scored for cell cycle phases as described by Macosko et al. (2015) using the phase-specific genes identified by Whitfield et al. (2002) (Supplemental Table S9). For each phase, the mean normalized expression of all phase-specific genes was first calculated for each cell, and then centered and scaled across all profiled cells. Phase scores were then centered and scaled within each cell. Cells were assigned to the phase for which they scored highest (Figure 1a and Supplemental Figure S1a).

For the differential expression analysis, only the top 50% of cells with the highest scores for each phase were retained (calculated individually for each cell line as shown in Supplemental Figure S1a). UMI counts were summed across all cells assigned to the same phase for each individual sample and replicate, and differential expression was calculated using the DESeq2 R package (Love et al. 2014) with default parameters, either for all NHA-CIC^{WT} vs NHA-CIC^{KO} samples or for all CIC^{WT} samples vs CIC^{KO} samples from a single cell line (NHA-CIC^{KO1} or NHA-CIC^{KO2}). Genes with a BH-corrected p-value < 0.1 and an absolute fold-change > 1.5 were considered to be significantly differentially expressed. To visualize these expression differences, DESeq2-normalized expression values were obtained using the

counts function with normalized = TRUE. By default, DESeq2 performs independent filtering based on mean expression across samples in order to select a set of genes for multiple test correction that maximizes the number of genes found at the specified false discovery rate (Love et al. 2014). Therefore, for each differential expression analysis, genes that were detected below the mean cutoff for that comparison were not analyzed (returned a corrected *p*-value of "NA"); these comparisons are indicated with "NC" (not calculated) in the relevant figures.

IP-MS

The IP-MS analyses of nuclear fractions from HEK293A cells using anti-endogenous CIC or anti-Myc (for N-Myc-CIC-S) antibodies (Supplemental Table S10) were performed as described previously (Chittaranjan et al. 2014) except using nuclear cell fractions (see Supplemental Methods for more detail). Three replicates were performed against endogenous CIC, and one experiment was performed against N-terminal MYC-fused CIC stably expressed in HEK293A cells. The IP-MS validation experiments performed in nuclear fractions of the NHA cell line were performed in triplicate, as were the matched IgG controls. See Supplemental Methods for methodological details.

Co-essentiality mapping and in silico genetic screening framework

DepMap public release version 20Q1 (DepMap 2020) was obtained from the DepMap platform portal (https://depmap.org/portal/download/). Co-essentiality mapping was performed using fitness effect scores (obtained from the Achilles_gene_effect.csv file) that were derived from normalized and copy number-corrected whole-genome CRISPR-Cas9 knockout screens targeting 18,332 genes performed in 739 cancer cell lines (Meyers et al. 2017; Dempster et al. 2019). The R statistical software (v4.0.2) was used to calculate and rank Pearson correlation coefficients between fitness scores of *CIC* and each targeted gene. The inflection point of the positive coefficient curve was calculated using the R package

RootsExtremaInflections (v1.2.1) (Christopoulos 2019). A pair of genes was considered co-essential if the BH-adjusted *p*-value was < 0.05 and the coefficient was > 0.178 (the inflection point).

CIC-mutant lines were identified using genomic data from 739 cancer cell lines, which were generated by the DepMap-Cancer Cell Lines Encyclopedia using a combination of whole-exome and whole-genome sequencing approaches (Ghandi et al. 2019). We took into account allele frequencies of single nucleotide variants (SNVs) and small insertions/deletions (indels), as well as copy number loss, to determine *CIC* zygosity for each cell line. We considered a mutation to be deleterious when the alteration was marked in DepMap as either De_novo_Start_OutOfFrame, Nonsense_Mutation, Nonstop_Mutation, Splice_Site, Frame_Shift_Del, Frame_Shift_Ins, Start_Codon_Del, Start_Codon_Ins, Stop_Codon_Del, or Stop_Codon_Ins in the Variant_Classification column of the mutations annotation file (CCLE_mutations.csv). From this file, we identified a mutation as homozygous if the allele call for the reference allele was zero. Otherwise, the mutation was considered heterozygous. We used a segment mean values threshold of < 0.25 from the copy number data (obtained from the CCLE_gene_cn.csv file) to determine whether there was a deep deletion at the *CIC* locus and a threshold of < 0.75 for partial deletion at the *CIC* locus. We identified two lines (HCC366 and JHUEM1) with homozygous deleterious *CIC* alterations (CIC^{HomDel}), five lines (REH, CCK81, HEC6, GP4D, and SISO) with potentially trans-heterozygous *CIC* mutations ($CIC^{T\text{-}HetDel}$; multiple heterozygous deleterious *CIC* mutations or a combination of partial copy number loss with heterozygous deleterious *CIC* mutation[s]), 53 lines with a single heterozygous deleterious *CIC* mutation or partial copy number loss (CIC^{HetDel}), and 557 lines with no *CIC* alterations (CIC^{WT}; Supplemental Table S6). The normalized TPM gene expression values were obtained from from the RNA-seq file (CCLE_expression.csv), and the normalized $\log_2$-like-transformed and mean-centered protein expression values were obtained from the proteomics file (protein_quant_current_normalized.csv). Protein values > 0 indicated protein counts above the mean across cell lines for which data were available (Nusinow and Gygi 2020).

We then compared the lethality probabilities of 18,332 genes (obtained from the Achilles_gene_dependency.csv file) generated by the DepMap CRISPR-Cas9 KO screens (Meyers et al. 2017; Dempster et al. 2019) to predict genetic interactors of *CIC*. The full description of the generation of lethality probabilities can be found in Meyers et al. (2017). We conducted pairwise Mann-Whitney U tests between *CIC* mutant and CIC^{WT} cell lines for all 18,332 genes screened using the R software. Candidate genetic interactors of *CIC* that were identified using CIC^{HomDel} mutant cell lines were defined as those with a Mann-Whitney U test p-value < 0.05, an absolute $\log_2$ fold-change of median probabilities > 1.5, and a median lethality probability > 0.5 in at least one group. Given that $CIC^{T\text{-}HetDel}$ lines are more heterogeneous compared to CIC^{HomDel} mutant cell lines, candidate genetic interactors derived from $CIC^{T\text{-}HetDel}$ lines were instead defined using a less stringent threshold of a Mann-Whitney U test p-value < 0.05 and a median lethality probability > 0.3 in at least one group. In both cases, known essential and non-essential genes (obtained from the common_essentials.csv and nonessentials.csv files, respectively) were filtered out.

Declarations

Ethics approval

Animal use was approved by the University of Calgary Animal Care Committee (protocol AC16-0266) in compliance with the Guidelines of the Canadian Council of Animal Care. The work presented here was approved by the UBC BC Cancer Research Ethics Board (H19-030103, H08-02838).

Availability of data and materials

scRNA-seq data have been deposited in the Gene Expression Omnibus (GEO; accession GSE193765). IP-MS data have been deposited to the ProteomeXchange Consortium via the Proteomics Identification (PRIDE) database (Perez-Riverol et al. 2019) (accession PXD030942).

Competing interests

SY is a member of the advisory boards of Amgen, AstraZeneca, Bayer, Incyte, and Roche. SAA is a co-founder of and consultant to Contextual Genomics Ltd and is on the advisory boards of Sangamo Biosciences and Repare Therapeutics. The remaining authors declare no competing interests.

Author contributions

MAM, YT, VGL and SC conceived and designed the experiments. SC, JS, and SYC produced the reagents and tools required for the *in vitro* experiments. STA and JAC provided the mouse brain tissue. SC, JS, SYC, SDL, YT, AG, DLT, and WRB performed most experiments. AM, CSH, and GBM performed and/or advised on the mass spectrometry experiments. YT, VGL, SDL, CSH, and SC analyzed the data. SC, VGL, and YT wrote initial drafts and VGL, YT, and MAM edited the manuscript. DLT, RDC, JAC, SAA, SMG, GBM, GJC, and SY provided ideas, discussions, and edits to the manuscript. MAM provided oversight. All authors have read and approved the final manuscript.

Acknowledgements

The authors thank the Sequencing, Bioinformatics, and Project Management teams at Canada's Michael Smith Genome Sciences Centre for expert technical contributions. We thank Dr. Michel Roberge and Dr. Phil Hieter for helpful edits and comments on early versions of the manuscript and Dr. G. Dawson for providing the HOG cell line. This study was supported in part by the Canadian Institutes of Health Research (CIHR; FDN-143288). We are especially grateful to Ms Donna Anderson for her generosity in supporting this project through the UBC Foundation. MAM gratefully acknowledges the support of BC Cancer, the BC Cancer Foundation, the Canada Research Chairs program, the Canada Foundation for Innovation (projects 20070, 30981, and 33408), Genome BC, Genome Canada, and the University of British Columbia (UBC). VGL was supported by a CIHR Vanier Canada Graduate Scholarship and a Killam Doctoral Scholarship. YT and VGL were supported by UBC 4-year fellowships.

References

Abbas T, Dutta A. 2009. p21 in cancer: intricate networks and multiple activities. *Nat Rev Cancer* **9**: 400–414.

Ahmad ST, Rogers AD, Chen MJ, Dixit R, Adnani L, Frankiw LS, Lawn SO, Blough MD, Alshehri M, Wu W, et al. 2019. Capicua regulates neural stem cell proliferation and lineage specification through control of Ets factors. *Nat Commun* **10**: 2000.

Alfonso-Pérez T, Hayward D, Holder J, Gruneberg U, Barr FA. 2019. MAD1-dependent recruitment of CDK1-CCNB1 to kinetochores promotes spindle checkpoint signaling. *J Cell Biol* **218**: 1108–1117.

Alpsoy A, Dykhuizen EC. 2018. Glioma tumor suppressor candidate region gene 1 (GLTSCR1) and its paralog GLTSCR1-like form SWI/SNF chromatin remodeling subcomplexes. *J Biol Chem* **293**: 3892–3903.

Antonescu CR, Owosho AA, Zhang L, Chen S, Deniz K, Huryn JM, Kao YC, Huang SC, Singer S, Tap W, et al. 2017. Sarcomas With CIC-rearrangements are a Distinct Pathologic Entity With Aggressive Outcome: A Clinicopathologic and Molecular Study of 115 Cases. *Am J Surg Pathol*. https://www.ncbi.nlm.nih.gov/pubmed/28346326.

Bairoch A, Apweiler R. 2000. The SWISS-PROT protein sequence database and its supplement TrEMBL in 2000. *Nucleic Acids Res* **28**: 45–48.

Bassermann F, Eichner R, Pagano M. 2014. The ubiquitin proteasome system—implications for cell cycle control and the targeted treatment of cancer. *Biochimica et Biophysica Acta (BBA)-Molecular Cell Research* **1843**: 150–162.

Bettegowda C, Agrawal N, Jiao Y, Sausen M, Wood LD, Hruban RH, Rodriguez FJ, Cahill DP, McLendon R, Riggins G, et al. 2011. Mutations in CIC and FUBP1 contribute to human oligodendroglioma. *Science* **333**: 1453–1455.

Bremm A, Komander D. 2011. Emerging roles for Lys11-linked polyubiquitin in cellular regulation. *Trends Biochem Sci* **36**: 355–363.

Brownlee PM, Chambers AL, Cloney R, Bianchi A, Downs JA. 2014. BAF180 promotes cohesion and prevents genome instability and aneuploidy. *Cell Rep* **6**: 973–981.

Bugler B, Quaranta M, Aressy B, Brezak M-C, Prevost G, Ducommun B. 2006. Genotoxic-activated G2-M checkpoint exit is dependent on CDC25B phosphatase expression. *Mol Cancer Ther* **5**: 1446–1451.

Bunda S, Heir P, Metcalf J, Li ASC, Agnihotri S, Pusch S, Yasin M, Li M, Burrell K, Mansouri S, et al. 2019. CIC protein instability contributes to tumorigenesis in glioblastoma. *Nat Commun* **10**: 661.

Cerami E, Gao J, Dogrusoz U, Gross BE, Sumer SO, Aksoy BA, Jacobsen A, Byrne CJ, Heuer ML, Larsson E, et al. 2012. The cBio cancer genomics portal: an open platform for exploring multidimensional cancer genomics data. *Cancer Discov* **2**: 401–404.

Chan AK, Pang JC, Chung NY, Li KK, Poon WS, Chan DT, Shi Z, Chen L, Zhou L, Ng HK. 2014. Loss of CIC and FUBP1 expressions are potential markers of shorter time to recurrence in oligodendroglial tumors. *Mod Pathol* **27**: 332–342.

Chittaranjan S, Chan S, Yang C, Yang KC, Chen V, Moradian A, Firme M, Song J, Go NE, Blough MD, et al. 2014. Mutations in CIC and IDH1 cooperatively regulate 2-hydroxyglutarate levels and cell clonogenicity. *Oncotarget* **5**: 7960–7979.

Choi N, Park J, Lee JS, Yoe J, Park GY, Kim E, Jeon H, Cho YM, Roh TY, Lee Y. 2015. miR-93/miR-106b/miR-375-CIC-CRABP1: a novel regulatory axis in prostate cancer progression. *Oncotarget* **6**: 23533–23547.

Christopoulos DT. 2019. RootsExtremaInflections: Finds Roots, Extrema and Inflection Points of a Curve. https://CRAN.R-project.org/package=RootsExtremaInflections.

Coisy-Quivy M, Disson O, Roure V, Muchardt C, Blanchard J-M, Dantonel J-C. 2006. Role for Brm in cell growth control. *Cancer Res* **66**: 5069–5076.

Cooper S. 2003. Rethinking synchronization of mammalian cells for cell cycle analysis. *Cell Mol Life Sci* **60**: 1099–1106.

Dempster JM, Rossen J, Kazachkova M, Pan J, Kugener G, Root DE, Tsherniak A. 2019. Extracting Biological Insights from the Project Achilles Genome-Scale CRISPR Screens in Cancer Cell Lines. 720243. https://www.biorxiv.org/content/10.1101/720243v1.abstract (Accessed July 31, 2020).

DepMap B. 2020. DepMap 20Q1 Public. http://dx.doi.org/10.6084/M9.FIGSHARE.11791698.V2.

Dykhuizen EC, Hargreaves DC, Miller EL, Cui K, Korshunov A, Kool M, Pfister S, Cho YJ, Zhao K, Crabtree GR. 2013. BAF complexes facilitate decatenation of DNA by topoisomerase IIalpha. *Nature* **497**: 624–627.

Erickson BK, Rose CM, Braun CR, Erickson AR, Knott J, McAlister GC, Wühr M, Paulo JA, Everley RA, Gygi SP. 2017. A Strategy to Combine Sample Multiplexing with Targeted Proteomics Assays for High-Throughput Protein Signature Characterization. *Mol Cell* **65**: 361–370.

Fedele M, Battista S, Manfioletti G, Croce CM, Giancotti V, Fusco A. 2001. Role of the high mobility group A proteins in human lipomas. *Carcinogenesis* **22**: 1583–1591.

Foijer F, Albacker LA, Bakker B, Spierings DC, Yue Y, Xie SZ, Davis S, Lutum-Jehle A, Takemoto D, Hare B, et al. 2017. Deletion of the MAD2L1 spindle assembly checkpoint gene is tolerated in mouse models of acute T-cell lymphoma and hepatocellular carcinoma. *Elife* **6**. http://dx.doi.org/10.7554/eLife.20873.

Foley EA, Kapoor TM. 2013. Microtubule attachment and spindle assembly checkpoint signalling at the kinetochore. *Nat Rev Mol Cell Biol* **14**: 25–37.

Frémont S, Gérard A, Galloux M, Janvier K, Karess RE, Berlioz-Torrent C. 2013. Beclin-1 is required for chromosome congression and proper outer kinetochore assembly. *EMBO Rep* **14**: 364–372.

Gao J, Aksoy BA, Dogrusoz U, Dresdner G, Gross B, Sumer SO, Sun Y, Jacobsen A, Sinha R, Larsson E, et al. 2013. Integrative analysis of complex cancer genomics and clinical profiles using the cBioPortal. *Sci Signal* **6**: l1.

Ghandi M, Huang FW, Jané-Valbuena J, Kryukov GV, Lo CC, McDonald ER 3rd, Barretina J, Gelfand ET, Bielski CM, Li H, et al. 2019. Next-generation characterization of the Cancer Cell Line Encyclopedia. *Nature* **569**: 503–508.

Giles KA, Gould CM, Achinger-Kawecka J, Page SG, Kafer GR, Rogers S, Luu P-L, Cesare AJ, Clark SJ, Taberlay PC. 2021. BRG1 knockdown inhibits proliferation through multiple cellular pathways in prostate cancer. *Clin Epigenetics* **13**: 37.

Gleize V, Alentorn A, Connen de Kerillis L, Labussiere M, Nadaradjane A, Mundwiller E, Ottolenghi C, Mangesius S, Rahimian A, Ducray F, et al. 2015. CIC inactivating mutations identify aggressive subset of 1p19q codeleted gliomas. *Ann Neurol* **78**: 355–374.

Gordon DJ, Resio B, Pellman D. 2012. Causes and consequences of aneuploidy in cancer. *Nat Rev Genet* **13**: 189–203.

Haidar A, Arekapudi S, DeMattia F, Abu-Isa E, Kraut M. 2015. High-grade undifferentiated small round cell sarcoma with t(4;19)(q35;q13.1) CIC-DUX4 fusion: emerging entities of soft tissue tumors with unique histopathologic features--a case report and literature review. *Am J Case Rep* **16**: 87–94.

Hashiba T, Yamashita T, Okada H, Nio K, Hayashi T, Asahina Y, Hayashi T, Terashima T, Iida N, Takatori H, et al. 2020. Inactivation of Transcriptional Repressor Capicua Confers Sorafenib Resistance in Human Hepatocellular Carcinoma. *Cell Mol Gastroenterol Hepatol* **10**: 269–285.

Hayward D, Alfonso-Pérez T, Cundell MJ, Hopkins M, Holder J, Bancroft J, Hutter LH, Novak B, Barr FA, Gruneberg U. 2019. CDK1-CCNB1 creates a spindle checkpoint–permissive state by enabling MPS1 kinetochore localization. *J Cell Biol* **218**: 1182–1199.

Heath EM, Chan SM, Minden MD, Murphy T, Shlush LI, Schimmer AD. 2017. Biological and clinical consequences of NPM1 mutations in AML. *Leukemia* **31**: 798–807.

Hsiao CJ, Tung P, Blischak JD, Burnett JE, Barr KA, Dey KK, Stephens M, Gilad Y. 2020. Characterizing and inferring quantitative cell cycle phase in single-cell RNA-seq data analysis. *Genome Res* **30**: 611–621.

Hughes CS, Foehr S, Garfield DA, Furlong EE, Steinmetz LM, Krijgsveld J. 2014. Ultrasensitive proteome analysis using paramagnetic bead technology. *Mol Syst Biol* **10**: 757.

Hughes CS, McConechy MK, Cochrane DR, Nazeran T, Karnezis AN, Huntsman DG, Morin GB. 2016. Quantitative Profiling of Single Formalin Fixed Tumour Sections: proteomics for translational research. *Scientific Reports* **6**. http://dx.doi.org/10.1038/srep34949.

Hwang I, Pan H, Yao J, Elemento O, Zheng H, Paik J. 2020. CIC is a critical regulator of neuronal differentiation. *JCI Insight* **5**. http://dx.doi.org/10.1172/jci.insight.135826.

Innis SM, Cabot B. 2020. GBAF, a small BAF sub-complex with big implications: a systematic review.

Epigenetics Chromatin **13**: 48.

Jiang N, Wang X, Jhanwar-Uniyal M, Darzynkiewicz Z, Dai W. 2006. Polo box domain of Plk3 functions as a centrosome localization signal, overexpression of which causes mitotic arrest, cytokinesis defects, and apoptosis. *J Biol Chem* **281**: 10577–10582.

Jimenez G, Shvartsman SY, Paroush Z. 2012. The Capicua repressor--a general sensor of RTK signaling in development and disease. *J Cell Sci* **125**: 1383–1391.

Jin Y, Ha N, Fores M, Xiang J, Glasser C, Maldera J, Jimenez G, Edgar BA. 2015. EGFR/Ras Signaling Controls Drosophila Intestinal Stem Cell Proliferation via Capicua-Regulated Genes. *PLoS Genet* **11**: e1005634.

Jullien D, Bugler B, Dozier C, Cazales M, Ducommun B. 2011. Identification of N-terminally truncated stable nuclear isoforms of CDC25B that are specifically involved in G2/M checkpoint recovery. *Cancer Res* **71**: 1968–1977.

Kalitsis P, Earle E, Fowler KJ, Choo KH. 2000. Bub3 gene disruption in mice reveals essential mitotic spindle checkpoint function during early embryogenesis. *Genes Dev* **14**: 2277–2282.

Käll L, Canterbury JD, Weston J, Noble WS, MacCoss MJ. 2007. Semi-supervised learning for peptide identification from shotgun proteomics datasets. *Nature Methods* **4**: 923–925. http://dx.doi.org/10.1038/nmeth1113.

LeBlanc VG, Firme M, Song J, Chan SY, Lee MH, Yip S, Chittaranjan S, Marra MA. 2017. Comparative transcriptome analysis of isogenic cell line models and primary cancers links CIC loss to activation of the MAPK signalling cascade. *J Pathol*. https://www.ncbi.nlm.nih.gov/pubmed/28295365.

Lee SD, Song J, LeBlanc VG, Marra MA. 2021. Integrative multi-omic analysis reveals neurodevelopmental gene dysregulation in CIC-knockout and IDH1 mutant cells. *J Pathol*. http://dx.doi.org/10.1002/path.5835.

Lee Y. 2020. Regulation and function of capicua in mammals. *Exp Mol Med* **52**: 531–537.

Le Gallic L, Virgilio L, Cohen P, Biteau B, Mavrothalassitis G. 2004. ERF nuclear shuttling, a continuous monitor of Erk activity that links it to cell cycle progression. *Mol Cell Biol* **24**: 1206–1218.

Liao S, Davoli T, Leng Y, Li MZ, Xu Q, Elledge SJ. 2017. A genetic interaction analysis identifies cancer drivers that modify EGFR dependency. *Genes Dev* **31**: 184–196.

Liu XS, Li H, Song B, Liu X. 2010. Polo-like kinase 1 phosphorylation of G2 and S-phase-expressed 1 protein is essential for p53 inactivation during G2 checkpoint recovery. *EMBO Rep* **11**: 626–632.

Liu Y, Chen S, Wang S, Soares F, Fischer M, Meng F, Du Z, Lin C, Meyer C, DeCaprio JA, et al. 2017. Transcriptional landscape of the human cell cycle. *Proc Natl Acad Sci U S A* **114**: 3473–3478.

Love MI, Huber W, Anders S. 2014. Moderated estimation of fold change and dispersion for RNA-seq data with DESeq2. *Genome Biol* **15**: 550.

Lun AT, Bach K, Marioni JC. 2016. Pooling across cells to normalize single-cell RNA sequencing data

with many zero counts. *Genome Biol* **17**: 75.

Macosko EZ, Basu A, Satija R, Nemesh J, Shekhar K, Goldman M, Tirosh I, Bialas AR, Kamitaki N, Martersteck EM, et al. 2015. Highly Parallel Genome-wide Expression Profiling of Individual Cells Using Nanoliter Droplets. *Cell* **161**: 1202–1214.

Meyers RM, Bryan JG, McFarland JM, Weir BA, Sizemore AE, Xu H, Dharia NV, Montgomery PG, Cowley GS, Pantel S, et al. 2017. Computational correction of copy number effect improves specificity of CRISPR-Cas9 essentiality screens in cancer cells. *Nat Genet* **49**: 1779–1784.

Michel BC, D'Avino AR, Cassel SH, Mashtalir N, McKenzie ZM, McBride MJ, Valencia AM, Zhou Q, Bocker M, Soares LMM, et al. 2018. A non-canonical SWI/SNF complex is a synthetic lethal target in cancers driven by BAF complex perturbation. *Nat Cell Biol* **20**: 1410–1420.

Mu R, Wang Y-B, Wu M, Yang Y, Song W, Li T, Zhang W-N, Tan B, Li A-L, Wang N, et al. 2014. Depletion of pre-mRNA splicing factor Cdc5L inhibits mitotic progression and triggers mitotic catastrophe. *Cell Death Dis* **5**: e1151.

Nijman SM. 2011. Synthetic lethality: general principles, utility and detection using genetic screens in human cells. *FEBS Lett* **585**: 1–6.

Nusinow DP, Gygi SP. 2020. A Guide to the Quantitative Proteomic Profiles of the Cancer Cell Line Encyclopedia. *bioRxiv* 2020.02.03.932384. https://www.biorxiv.org/content/10.1101/2020.02.03.932384v1.full.pdf+html (Accessed April 15, 2020).

Nusinow DP, Szpyt J, Ghandi M, Rose CM, McDonald ER 3rd, Kalocsay M, Jané-Valbuena J, Gelfand E, Schweppe DK, Jedrychowski M, et al. 2020. Quantitative Proteomics of the Cancer Cell Line Encyclopedia. *Cell* **180**: 387–402.e16.

Okimoto RA, Breitenbuecher F, Olivas VR, Wu W, Gini B, Hofree M, Asthana S, Hrustanovic G, Flanagan J, Tulpule A, et al. 2017. Inactivation of Capicua drives cancer metastasis. *Nat Genet* **49**: 87–96.

Okuda M, Horn HF, Tarapore P, Tokuyama Y, Smulian AG, Chan PK, Knudsen ES, Hofmann IA, Snyder JD, Bove KE, et al. 2000. Nucleophosmin/B23 is a target of CDK2/cyclin E in centrosome duplication. *Cell* **103**: 127–140.

Pan J, Meyers RM, Michel BC, Mashtalir N, Sizemore AE, Wells JN, Cassel SH, Vazquez F, Weir BA, Hahn WC, et al. 2018. Interrogation of Mammalian Protein Complex Structure, Function, and Membership Using Genome-Scale Fitness Screens. *Cell Syst* **6**: 555–568.e7.

Perez-Riverol Y, Csordas A, Bai J, Bernal-Llinares M, Hewapathirana S, Kundu DJ, Inuganti A, Griss J, Mayer G, Eisenacher M, et al. 2019. The PRIDE database and related tools and resources in 2019: improving support for quantification data. *Nucleic Acids Res* **47**: D442–D450.

Perkins DN, Pappin DJ, Creasy DM, Cottrell JS. 1999. Probability-based protein identification by searching sequence databases using mass spectrometry data. *Electrophoresis* **20**: 3551–3567.

Post GR, Dawson G. 1992. Characterization of a cell line derived from a human oligodendroglioma. *Mol Chem Neuropathol* **16**: 303–317.

Rappsilber J, Ishihama Y, Mann M. 2003. Stop and Go Extraction Tips for Matrix-Assisted Laser Desorption/Ionization, Nanoelectrospray, and LC/MS Sample Pretreatment in Proteomics. *Analytical Chemistry* **75**: 663–670. http://dx.doi.org/10.1021/ac026117i.

R Core Team. 2020. *R: A Language and Environment for Statistical Computing*. R Foundation for Statistical Computing, Vienna, Austria https://www.R-project.org/.

Ricke RM, Jeganathan KB, van Deursen JM. 2011. Bub1 overexpression induces aneuploidy and tumor formation through Aurora B kinase hyperactivation. *J Cell Biol* **193**: 1049–1064.

Seki A, Coppinger JA, Jang C-Y, Yates JR, Fang G. 2008. Bora and the kinase Aurora a cooperatively activate the kinase Plk1 and control mitotic entry. *Science* **320**: 1655–1658.

Simon-Carrasco L, Grana O, Salmon M, Jacob HKC, Gutierrez A, Jimenez G, Drosten M, Barbacid M. 2017. Inactivation of Capicua in adult mice causes T-cell lymphoblastic lymphoma. *Genes Dev*. https://www.ncbi.nlm.nih.gov/pubmed/28827401.

Simón-Carrasco L, Jiménez G, Barbacid M, Drosten M. 2018. The Capicua tumor suppressor: a gatekeeper of Ras signaling in development and cancer. *Cell Cycle* **17**: 702–711.

Söderberg O, Gullberg M, Jarvius M, Ridderstråle K, Leuchowius K-J, Jarvius J, Wester K, Hydbring P, Bahram F, Larsson L-G, et al. 2006. Direct observation of individual endogenous protein complexes in situ by proximity ligation. *Nat Methods* **3**: 995–1000.

Sonoda Y, Ozawa T, Hirose Y, Aldape KD, McMahon M, Berger MS, Pieper RO. 2001. Formation of intracranial tumors by genetically modified human astrocytes defines four pathways critical in the development of human anaplastic astrocytoma. *Cancer Res* **61**: 4956–4960.

Specht K, Sung YS, Zhang L, Richter GH, Fletcher CD, Antonescu CR. 2014. Distinct transcriptional signature and immunoprofile of CIC-DUX4 fusion-positive round cell tumors compared to EWSR1-rearranged Ewing sarcomas: further evidence toward distinct pathologic entities. *Genes Chromosomes Cancer* **53**: 622–633.

Spivak M, Weston J, Bottou L, Käll L, Noble WS. 2009. Improvements to the Percolator Algorithm for Peptide Identification from Shotgun Proteomics Data Sets. *Journal of Proteome Research* **8**: 3737–3745. http://dx.doi.org/10.1021/pr801109k.

St-Denis NA, Litchfield DW. 2009. Protein Kinase CK2 in Health and Disease. *Cell Mol Life Sci* **66**: 1817–1829.

Tan Q, Brunetti L, Rousseaux MWC, Lu HC, Wan YW, Revelli JP, Liu Z, Goodell MA, Zoghbi HY. 2018. Loss of Capicua alters early T cell development and predisposes mice to T cell lymphoblastic leukemia/lymphoma. *Proc Natl Acad Sci U S A*. https://www.ncbi.nlm.nih.gov/pubmed/29382756.

The Cancer Genome Atlas Research Network,. 2014. Comprehensive molecular characterization of

gastric adenocarcinoma. *Nature* **513**: 202–209.

The Cancer Genome Atlas Research Network,. 2013. Integrated genomic characterization of endometrial carcinoma. *Nature* **497**: 67–73.

UniProt Consortium. 2021. UniProt: the universal protein knowledgebase in 2021. *Nucleic Acids Res* **49**: D480–D489.

van Leeuwen J, Boone C, Andrews BJ. 2017. Mapping a diversity of genetic interactions in yeast. *Curr Opin Syst Biol* **6**: 14–21.

Vignali R, Marracci S. 2020. HMGA Genes and Proteins in Development and Evolution. *Int J Mol Sci* **21**. http://dx.doi.org/10.3390/ijms21020654.

Wang B, Krall EB, Aguirre AJ, Kim M, Widlund HR, Doshi MB, Sicinska E, Sulahian R, Goodale A, Cowley GS, et al. 2017. ATXN1L, CIC, and ETS Transcription Factors Modulate Sensitivity to MAPK Pathway Inhibition. *Cell Rep* **18**: 1543–1557.

Wang Q, Xie S, Chen J, Fukasawa K, Naik U, Traganos F, Darzynkiewicz Z, Jhanwar-Uniyal M, Dai W. 2002. Cell cycle arrest and apoptosis induced by human Polo-like kinase 3 is mediated through perturbation of microtubule integrity. *Mol Cell Biol* **22**: 3450–3459.

Warren CD, Michelle Brady D, Johnston RC, Hanna JS, Hardwick KG, Spencer FA. 2002. Distinct Chromosome Segregation Roles for Spindle Checkpoint Proteins. *Mol Biol Cell* **13**: 3029–3041.

Weissmann S, Cloos PA, Sidoli S, Jensen ON, Pollard S, Helin K. 2018. The Tumor Suppressor CIC Directly Regulates MAPK Pathway Genes via Histone Deacetylation. *Cancer Res* **78**: 4114–4125.

Whitfield ML, Sherlock G, Saldanha AJ, Murray JI, Ball CA, Alexander KE, Matese JC, Perou CM, Hurt MM, Brown PO, et al. 2002. Identification of genes periodically expressed in the human cell cycle and their expression in tumors. *Mol Biol Cell* **13**: 1977–2000.

Wong D, Lounsbury K, Lum A, Song J, Chan S, LeBlanc V, Chittaranjan S, Marra M, Yip S. 2019. Transcriptomic analysis of CIC and ATXN1L reveal a functional relationship exploited by cancer. *Oncogene* **38**: 273–290.

Wu T, Hu E, Xu S, Chen M, Guo P, Dai Z, Feng T, Zhou L, Tang W, Zhan L, et al. 2021. clusterProfiler 4.0: A universal enrichment tool for interpreting omics data. *Innovation (N Y)* **2**: 100141.

Xue Y, Canman JC, Lee CS, Nie Z, Yang D, Moreno GT, Young MK, Salmon ED, Wang W. 2000. The human SWI/SNF-B chromatin-remodeling complex is related to yeast rsc and localizes at kinetochores of mitotic chromosomes. *Proc Natl Acad Sci U S A* **97**: 13015–13020.

Yip S, Butterfield YS, Morozova O, Chittaranjan S, Blough MD, An J, Birol I, Chesnelong C, Chiu R, Chuah E, et al. 2012. Concurrent CIC mutations, IDH mutations, and 1p/19q loss distinguish oligodendrogliomas from other cancers. *J Pathol* **226**: 7–16.

You SY, Park YS, Jeon H-J, Cho D-H, Jeon HB, Kim SH, Chang JW, Kim J-S, Oh JS. 2016. Beclin-1 knockdown shows abscission failure but not autophagy defect during oocyte meiotic maturation. *Cell*

Cycle **15**: 1611–1619.

Zhang T, Zhou Y, Qi S-T, Wang Z-B, Qian W-P, Ouyang Y-C, Shen W, Schatten H, Sun Q-Y. 2015. Nuf2 is required for chromosome segregation during mouse oocyte meiotic maturation. *Cell Cycle* **14**: 2701–2710.

Zhou Y, Zhou B, Pache L, Chang M, Khodabakhshi AH, Tanaseichuk O, Benner C, Chanda SK. 2019. Metascape provides a biologist-oriented resource for the analysis of systems-level datasets. *Nat Commun* **10**: 1523.

Zimmerman WC, Erikson RL. 2007. Finding Plk3. *Cell Cycle* **6**: 1314–1318.

Zolg DP, Wilhelm M, Schnatbaum K, Zerweck J, Knaute T, Delanghe B, Bailey DJ, Gessulat S, Ehrlich H-C, Weininger M, et al. 2017. Building ProteomeTools based on a complete synthetic human proteome. *Nature Methods* **14**: 259–262. http://dx.doi.org/10.1038/nmeth.4153.